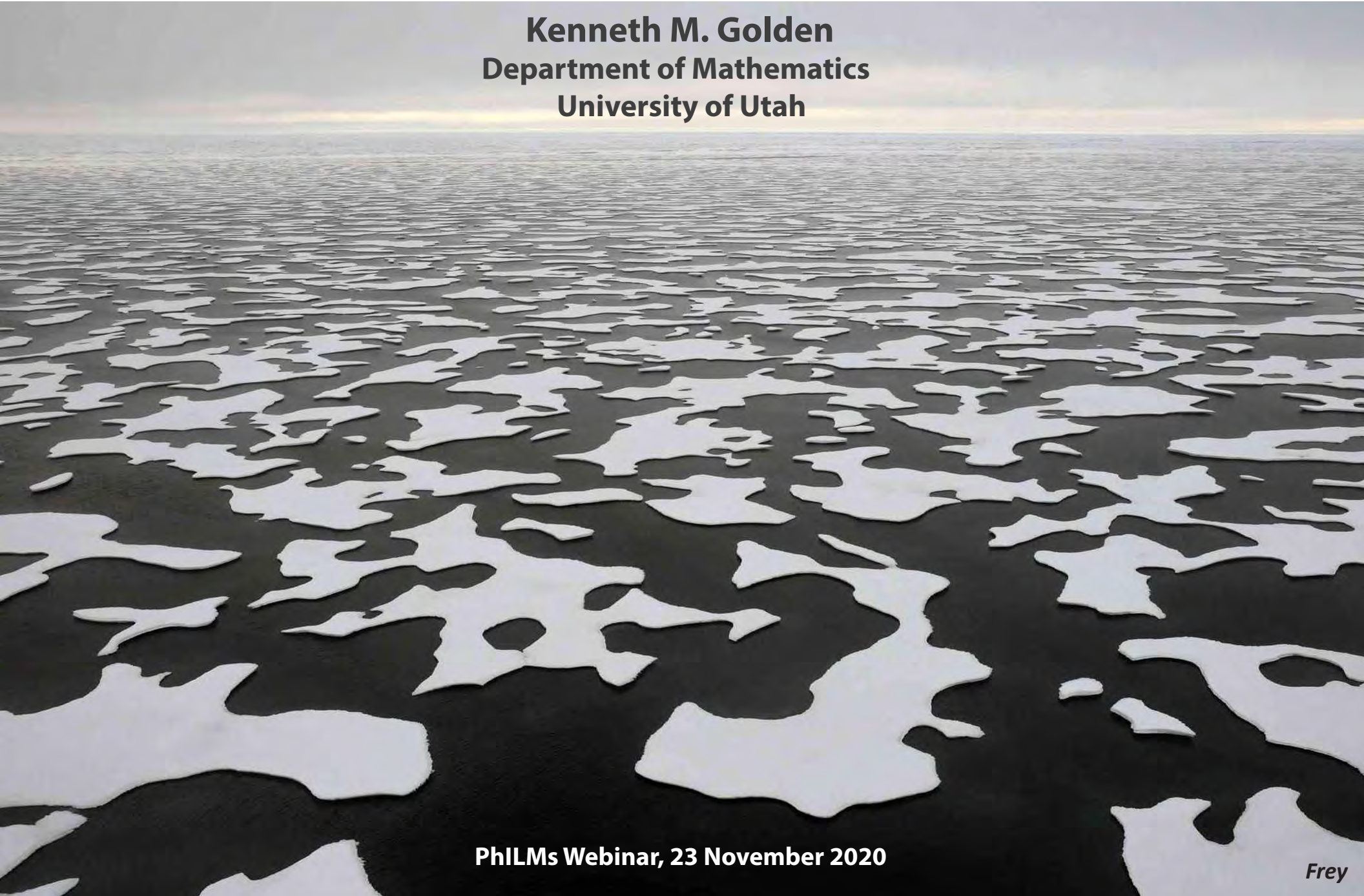


Modeling Sea Ice as a Multiscale Composite Material

Kenneth M. Golden
Department of Mathematics
University of Utah



SEA ICE covers ~12% of Earth's ocean surface

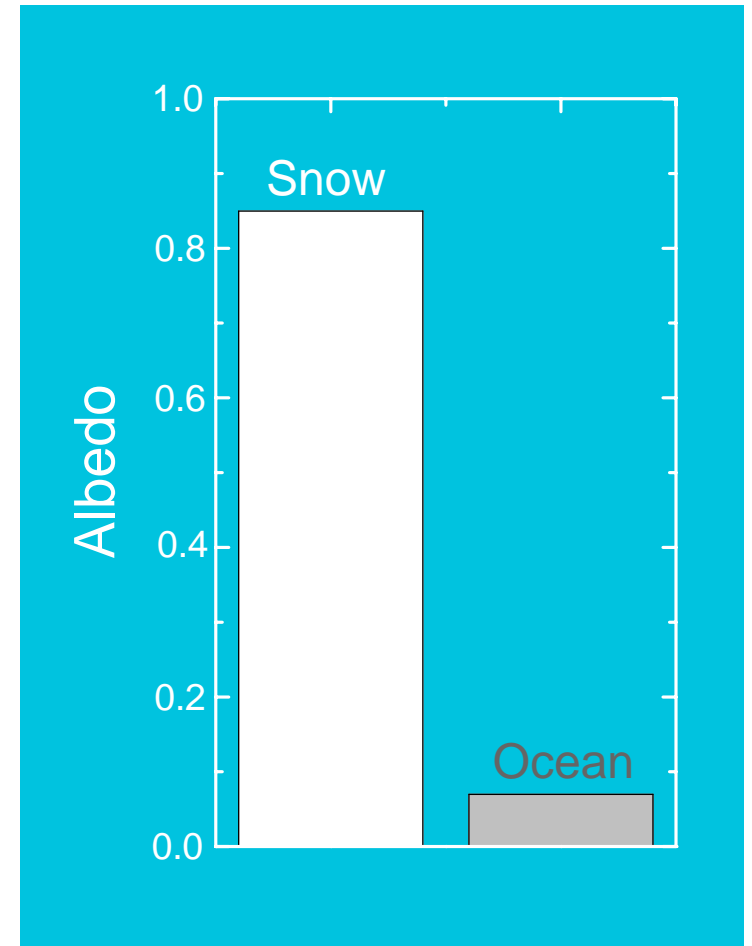
- boundary between ocean and atmosphere
- mediates exchange of heat, gases, momentum
- global ocean circulation
- hosts rich ecosystem
- indicator of **climate change**



polar ice caps critical to global climate in reflecting incoming solar radiation



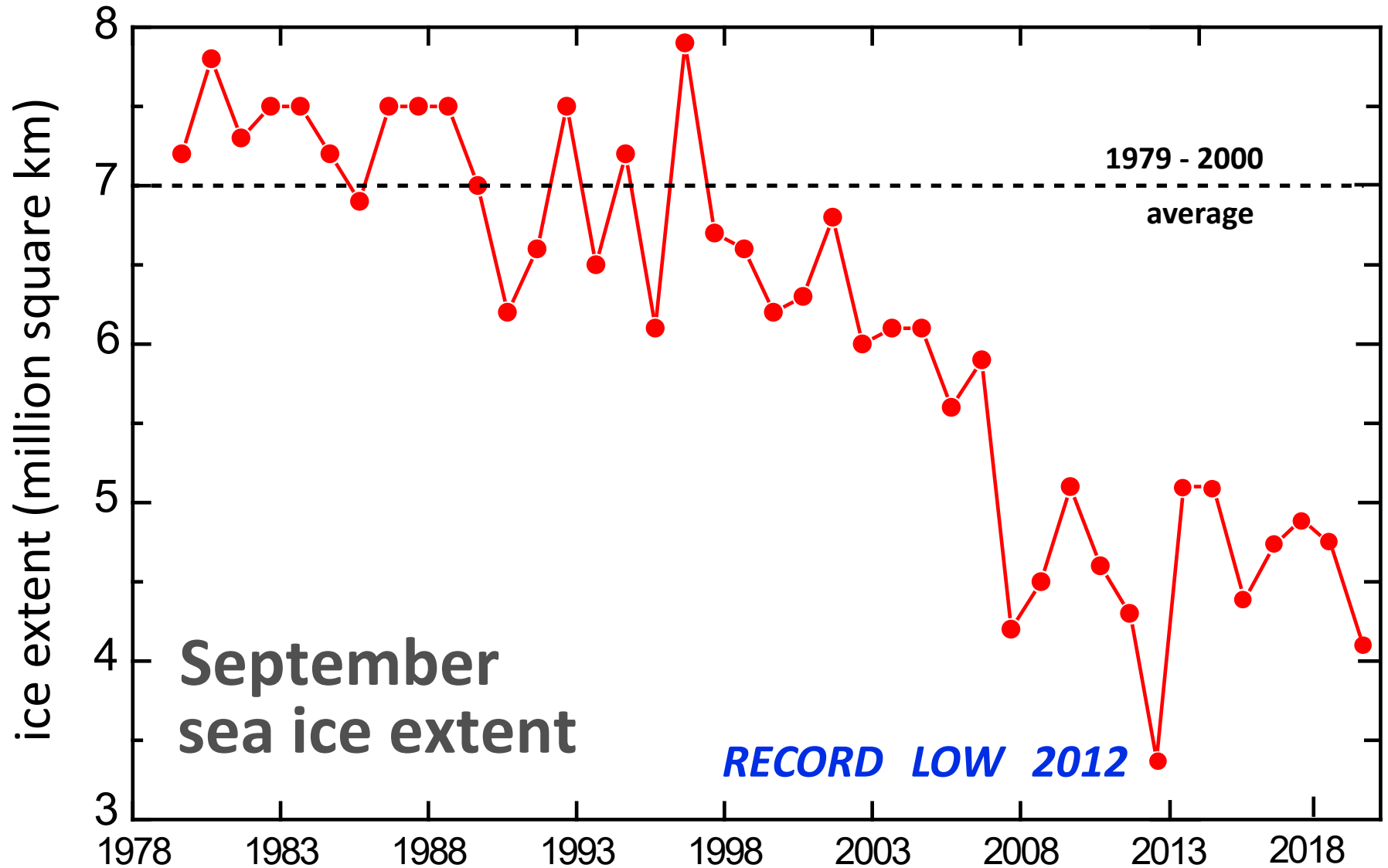
white snow and ice
reflect



dark water and land
absorb

$$\text{albedo } \alpha = \frac{\text{reflected sunlight}}{\text{incident sunlight}}$$

the summer Arctic sea ice pack is melting



Change in Arctic Sea Ice Extent

September 1980 -- 7.8 million km²

September 2012 -- 3.4 million km²



*recent losses
in comparison to
the United States*

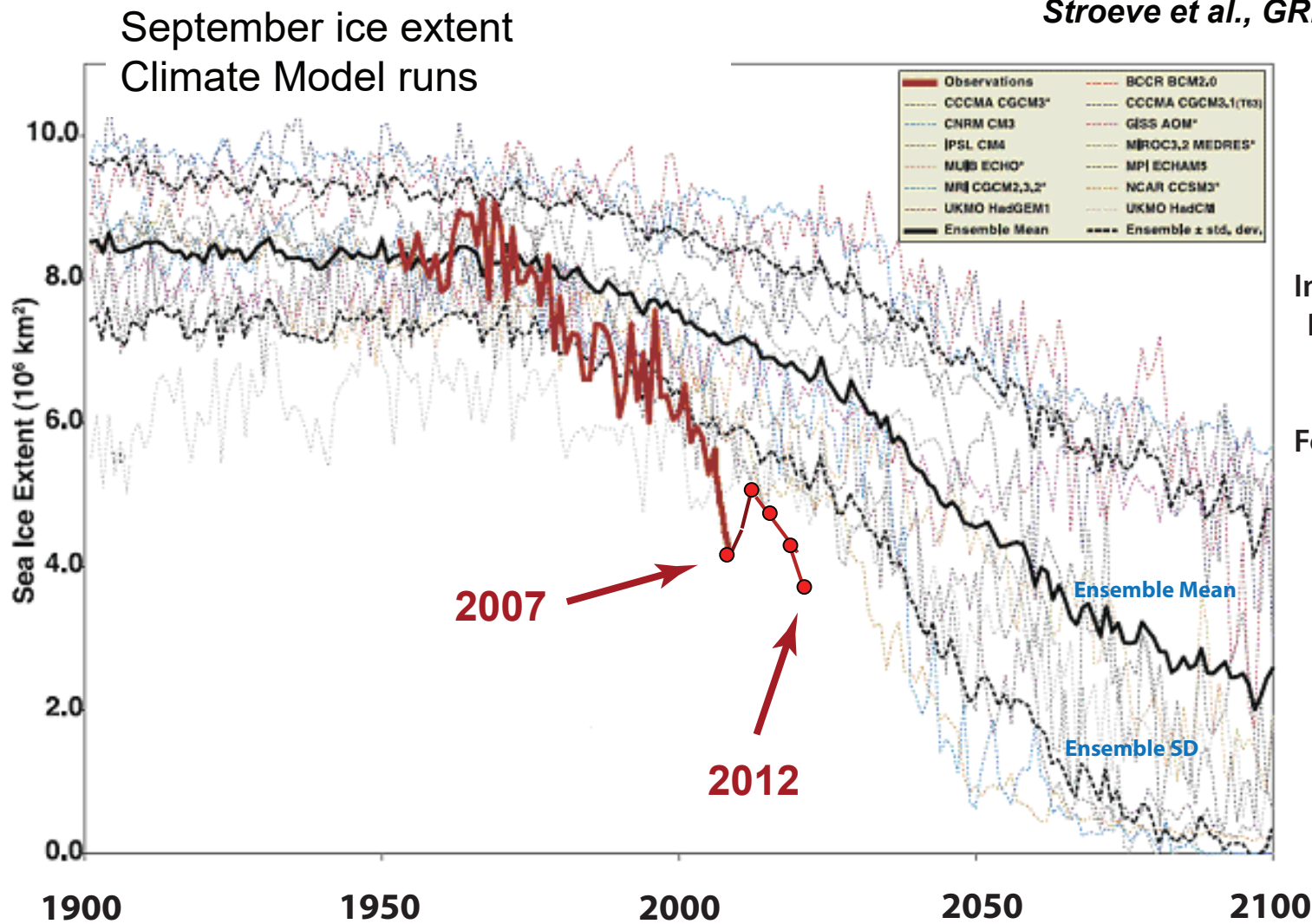
Perovich



Arctic sea ice decline: faster than predicted by climate models

Stroeve et al., GRL, 2007

Stroeve et al., GRL, 2012



IPCC AR4
Models

Intergovernmental
Panel on Climate
Change (IPCC)

Fourth Assessment
AR4, 2007

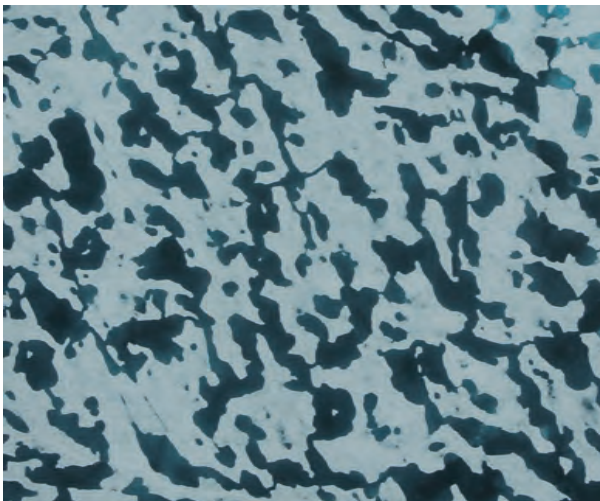
challenge

represent sea ice more realistically in climate models

account for key processes

such as melt pond evolution

*How do patterns of
dark and light evolve?*



Impact of melt ponds on Arctic sea ice
simulations from 1990 to 2007

Flocco, Schroeder, Feltham, Hunke, JGR Oceans 2012

**For simulations with ponds
September ice volume is nearly 40% lower.**

... and other sub-grid scale structures and processes

linkage of scales

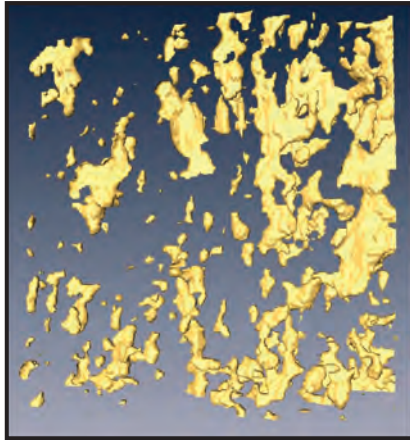
Sea Ice is a Multiscale Composite Material

sea ice microstructure

brine inclusions

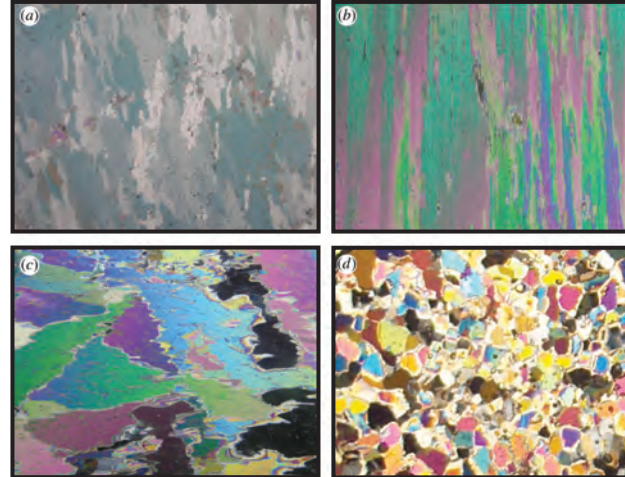


Weeks & Assur 1969



H. Eicken
Golden et al. GRL 2007

polycrystals



Gully et al. Proc. Roy. Soc. A 2015

brine channels



D. Cole



K. Golden

millimeters

centimeters

sea ice mesostructure

Arctic melt ponds



K. Frey

Antarctic pressure ridges



K. Golden

sea ice macrostructure

sea ice floes



J. Weller

sea ice pack

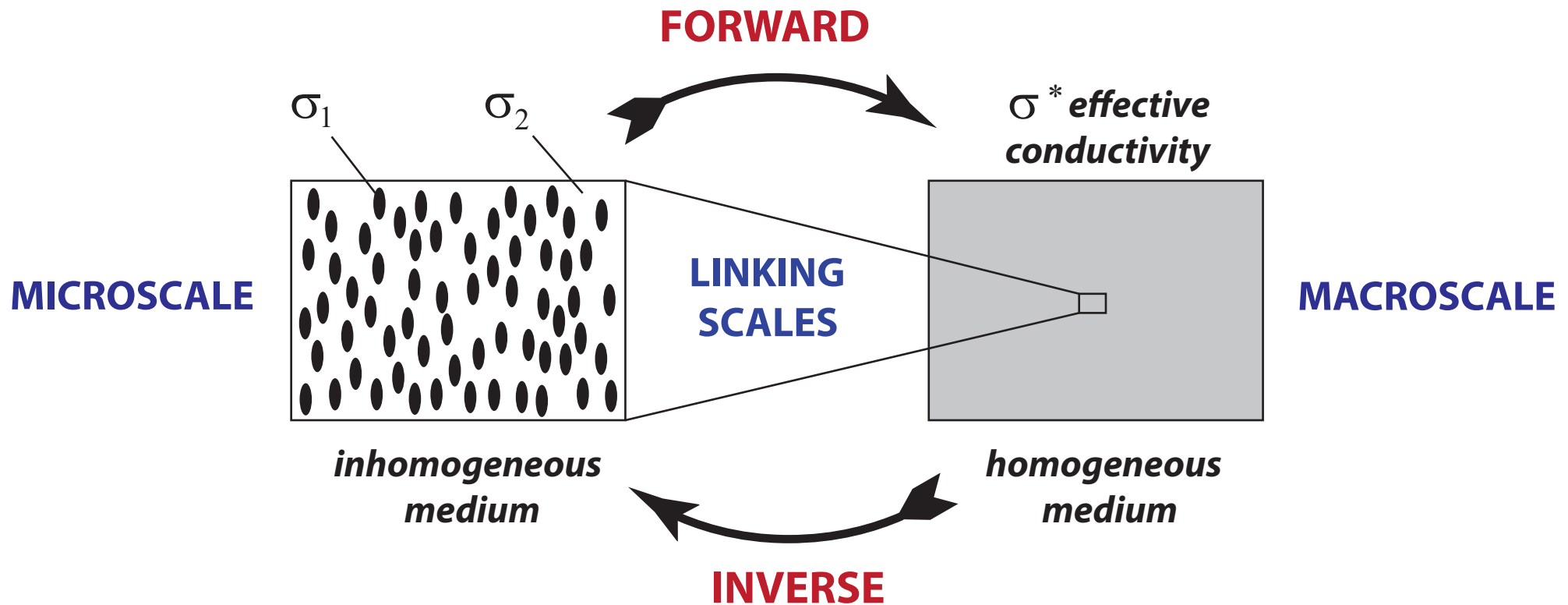


NASA

meters

kilometers

HOMOGENIZATION for Composite Materials



Maxwell 1873 : effective conductivity of a dilute suspension of spheres

Einstein 1906 : effective viscosity of a dilute suspension of rigid spheres in a fluid

*Wiener 1912 : arithmetic and harmonic mean **bounds** on effective conductivity*

*Hashin and Shtrikman 1962 : variational **bounds** on effective conductivity*

widespread use of composites in late 20th century due in large part to advances in mathematically predicting their effective properties

What is this talk about? **homogenization for multiscale composites**

the role of “microstructure” in determining sea ice effective properties

Using methods of **homogenization and statistical physics** to LINK SCALES in the sea ice system ... compute effective behavior on scales relevant to coarse-grained sea ice and climate models, process studies, ...

MICROSCALE: brine + polycrystalline structure; EM and fluid transport

MESOSCALE: advection diffusion, thermal transport, waves, melt ponds

MACROSCALE: ice transport, MIZ width and location, low order models

A tour of Stieltjes integrals in the study of sea ice and its role in climate.

Solving problems in physics of sea ice drives advances in theory of composite materials.

cross - pollination

**bone, stealthy coatings
magnets, rat brains, RMT**

How do scales interact in the sea ice system?



basin scale -
grid scale
albedo

NASA

Linking Scales

km
scale
melt
ponds



km
scale
melt
ponds



Perovich

Linking

Scales

mm
scale
brine
inclusions



meter
scale
snow
topography



sea ice microphysics

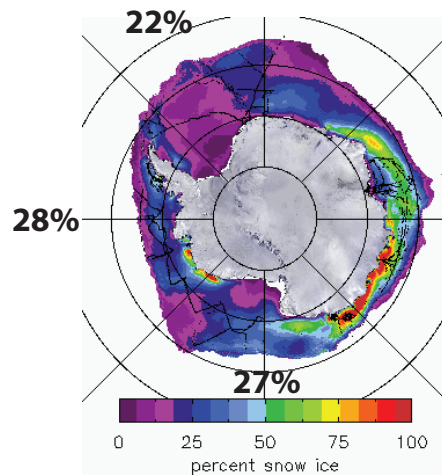
fluid transport

fluid flow through the porous microstructure of sea ice governs key processes in polar climate and ecosystems

evolution of Arctic melt ponds and sea ice albedo



nutrient flux for algal communities



T. Maksym and T. Markus, 2008

*Antarctic surface flooding
and snow-ice formation*

September
snow-ice
estimates

- evolution of salinity profiles
- ocean-ice-air exchanges of heat, CO₂

fluid permeability of a porous medium



how much water gets through the sample per unit time?

Darcy's Law

for slow viscous flow in a porous medium

averaged
fluid velocity

pressure
gradient

$$\mathbf{v} = -\frac{\mathbf{k}}{\eta} \nabla p$$

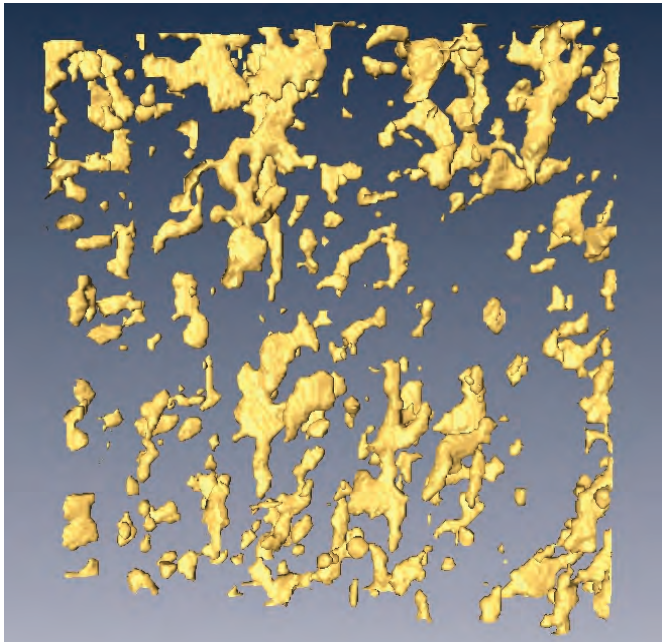
viscosity

\mathbf{k} = fluid permeability tensor

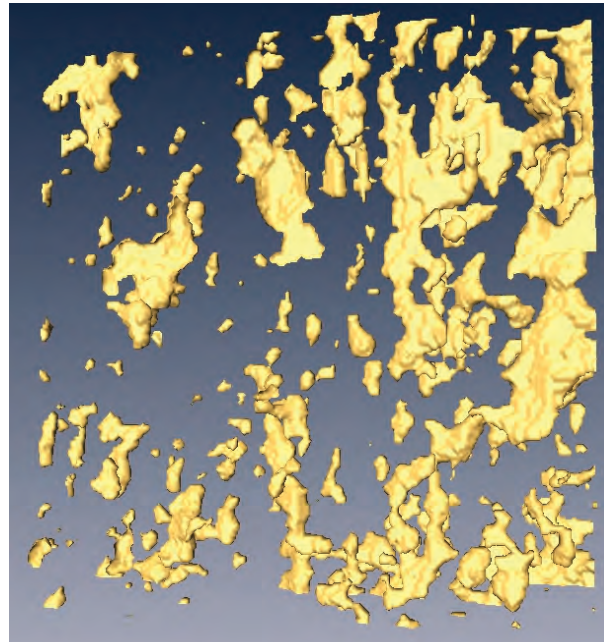
HOMOGENIZATION

mathematics for analyzing effective behavior of heterogeneous systems

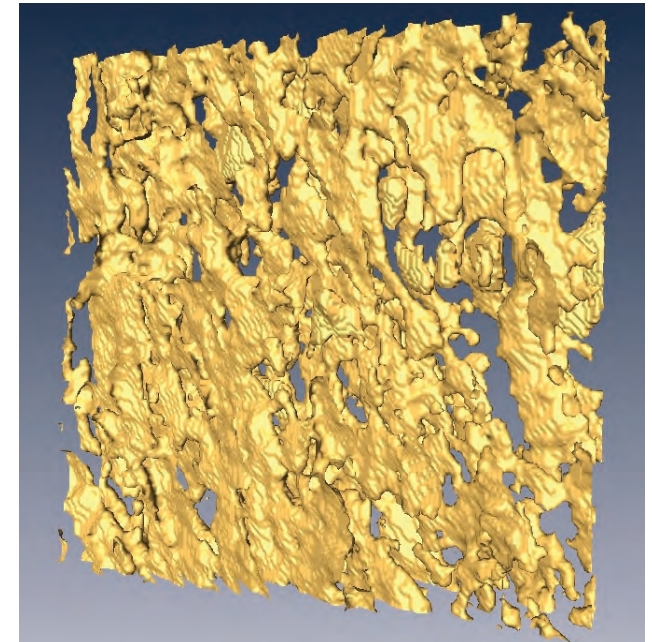
brine volume fraction and **connectivity** increase with temperature



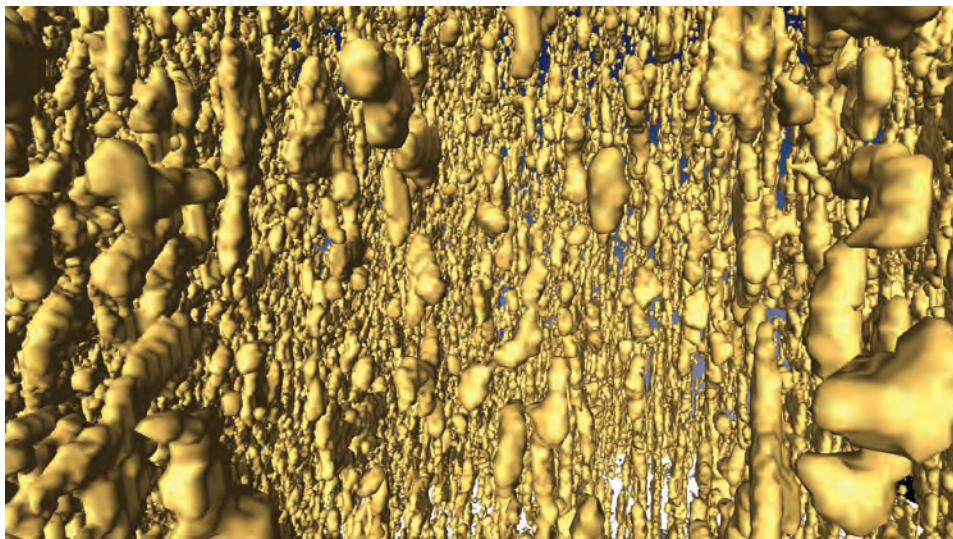
$T = -15\text{ }^{\circ}\text{C}, \phi = 0.033$



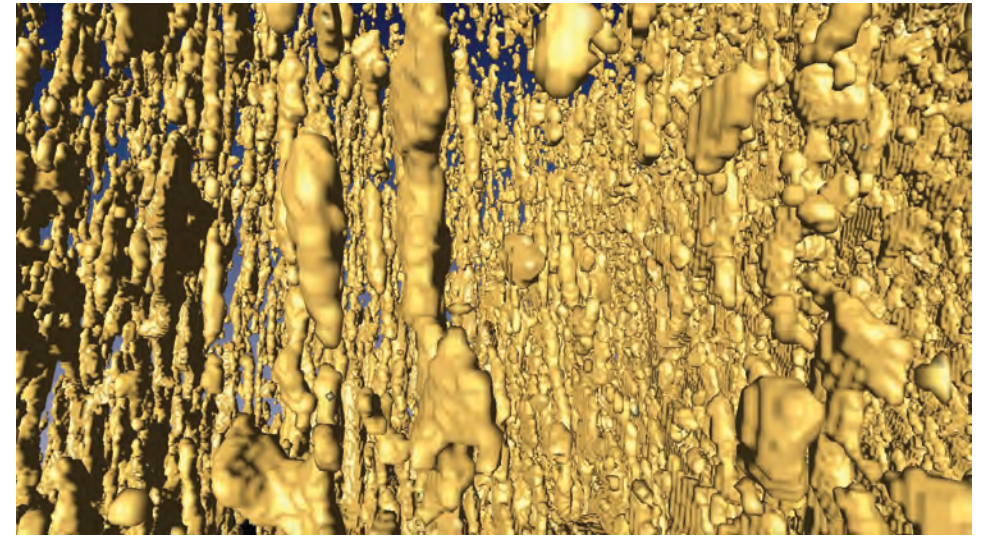
$T = -6\text{ }^{\circ}\text{C}, \phi = 0.075$



$T = -3\text{ }^{\circ}\text{C}, \phi = 0.143$

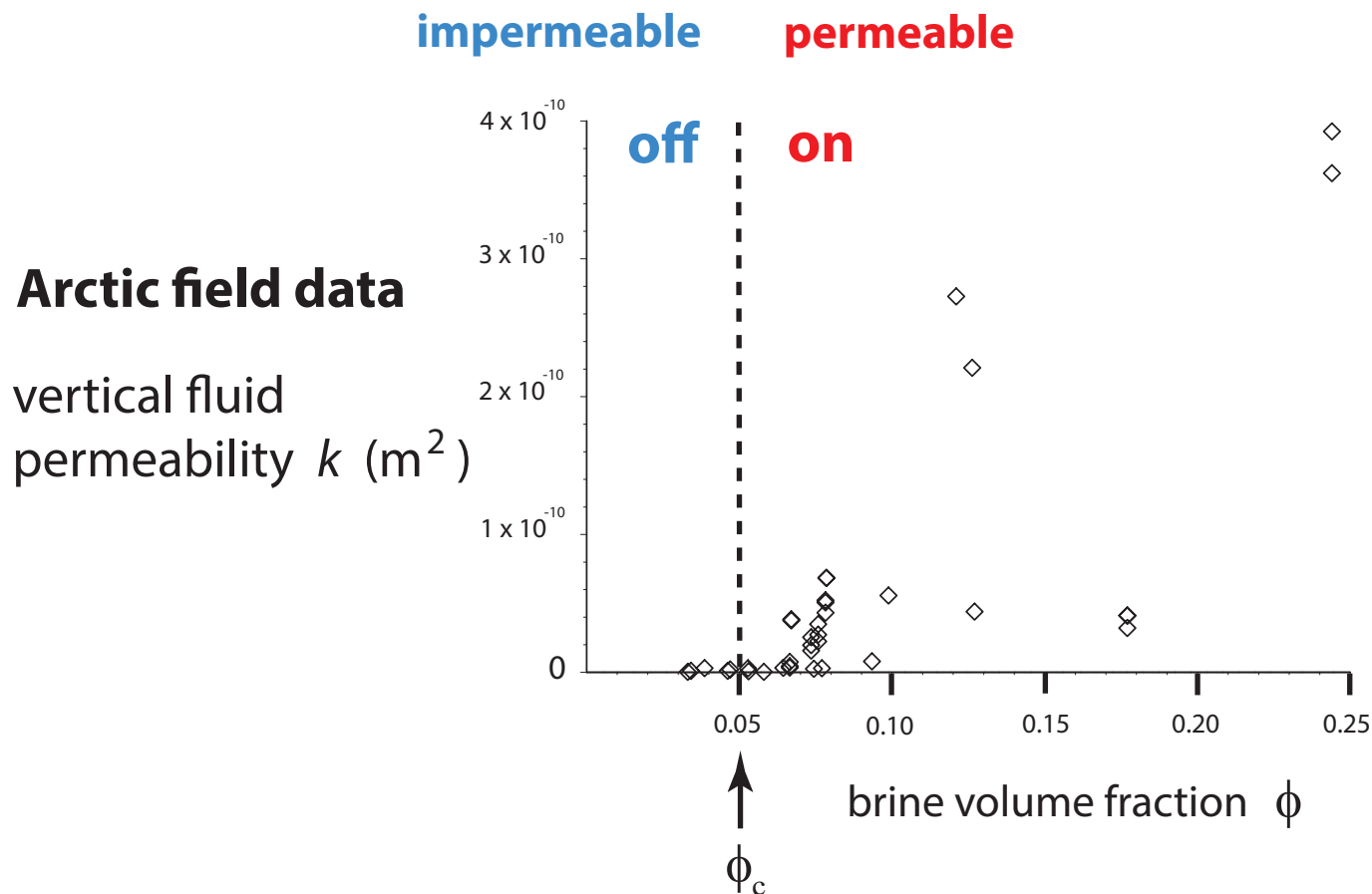


$T = -8\text{ }^{\circ}\text{C}, \phi = 0.057$



$T = -4\text{ }^{\circ}\text{C}, \phi = 0.113$

Critical behavior of fluid transport in sea ice



**“on - off” switch
for fluid flow**

critical brine volume fraction $\phi_c \approx 5\%$ \longleftrightarrow $T_c \approx -5^\circ \text{C}$, $S \approx 5 \text{ ppt}$

RULE OF FIVES

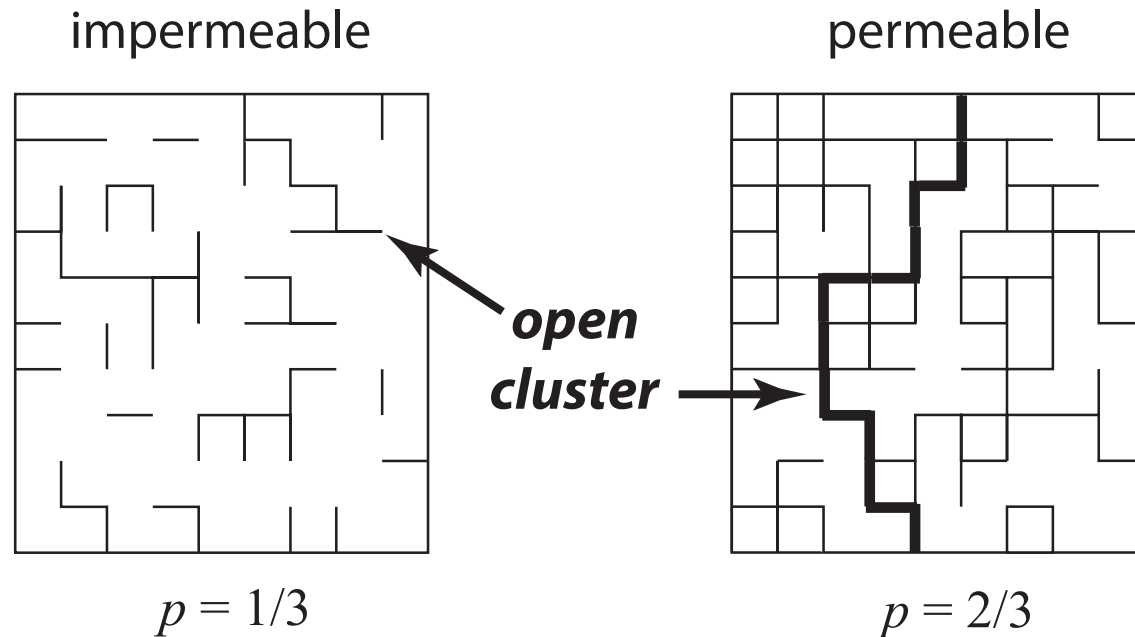
Golden, Ackley, Lytle Science 1998

Golden, Eicken, Heaton, Miner, Pringle, Zhu GRL 2007

Pringle, Miner, Eicken, Golden J. Geophys. Res. 2009

percolation theory

probabilistic theory of connectedness



bond \longrightarrow *open* with probability p
closed with probability $1-p$

percolation threshold

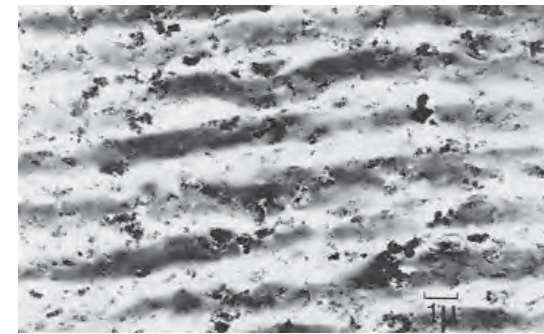
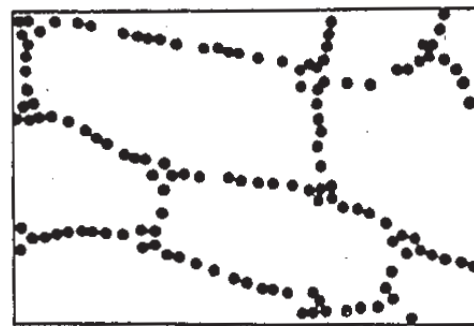
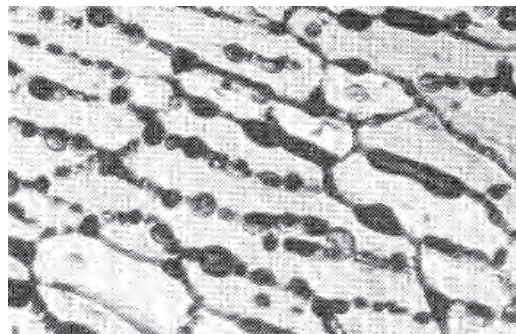
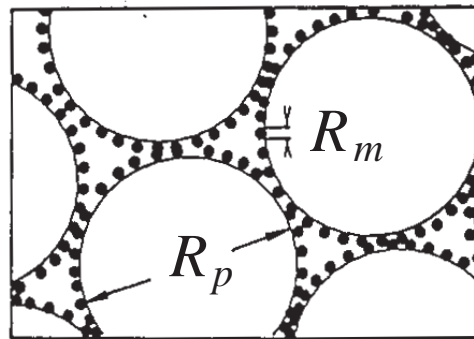
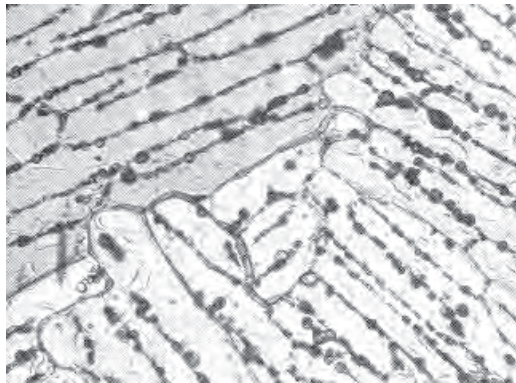
$$p_c = 1/2 \quad \text{for } d = 2$$

smallest p for which there is an infinite open cluster

Continuum percolation model for **stealthy** materials applied to sea ice microstructure explains **Rule of Fives** and Antarctic data on **ice production** and **algal growth**

$$\phi_c \approx 5\%$$

Golden, Ackley, Lytle, *Science*, 1998



sea ice

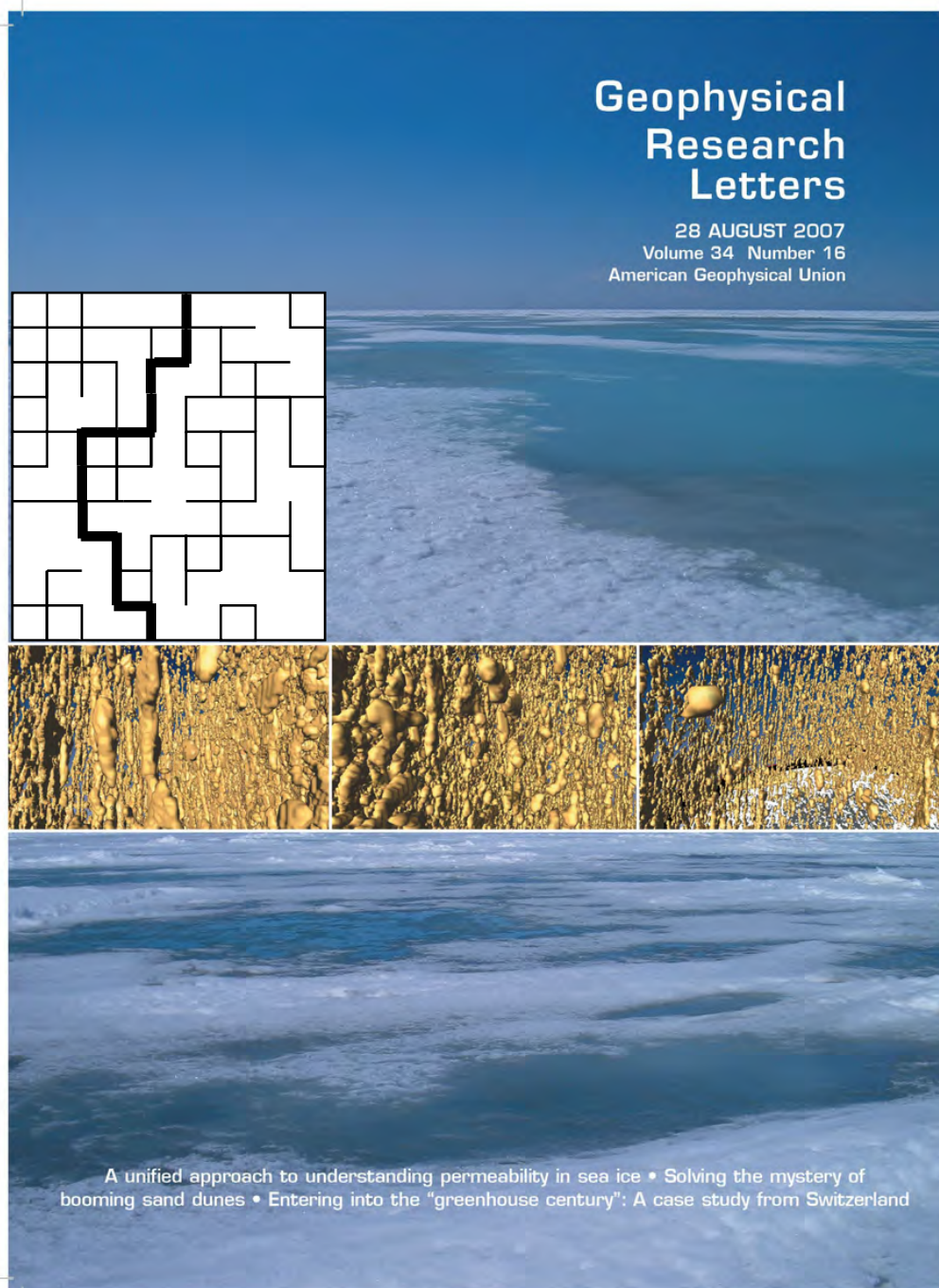
compressed powder

radar absorbing composite

sea ice is radar absorbing

Thermal evolution of permeability and microstructure in sea ice

Golden, Eicken, Heaton, Miner, Pringle, Zhu, *Geophysical Research Letters* 2007



micro-scale
controls
macro-scale
processes

percolation theory

$$k(\phi) = k_0 (\phi - 0.05)^t$$

t ← critical exponent

$$k_0 = 3 \times 10^{-8} \text{ m}^2$$

hierarchical model
network model
rigorous bounds

agree closely with
field data

X-ray tomography for
brine inclusions

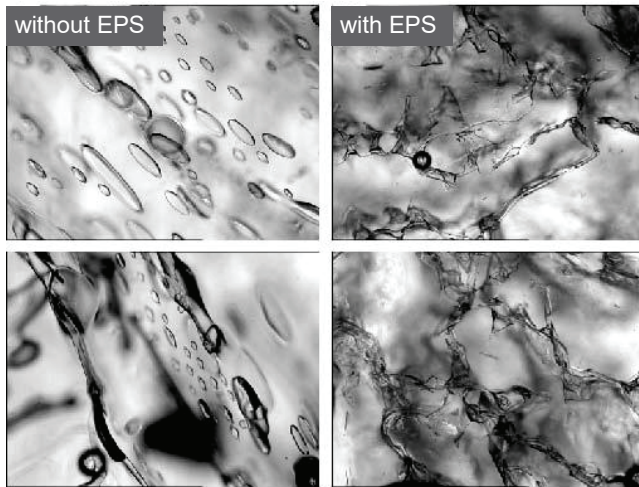
unprecedented look
at thermal evolution
of brine phase and
its connectivity

confirms rule of fives

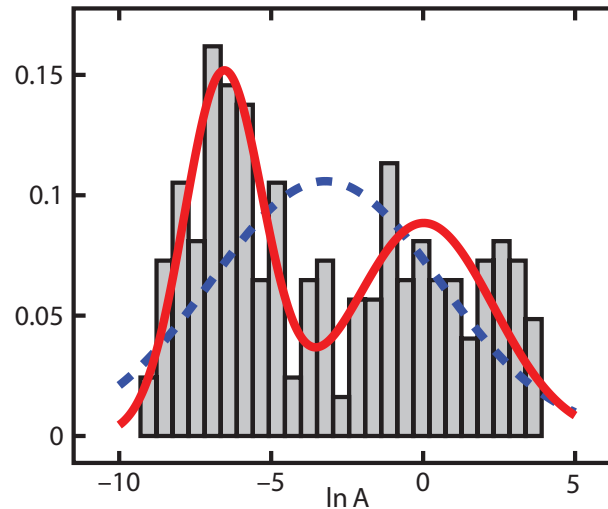
Pringle, Miner, Eicken, Golden
J. Geophys. Res. 2009

Sea ice algae secrete extracellular polymeric substances (EPS) affecting evolution of brine microstructure.

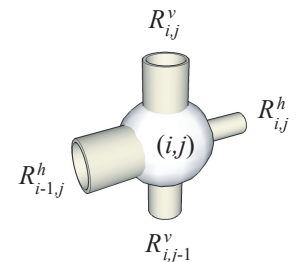
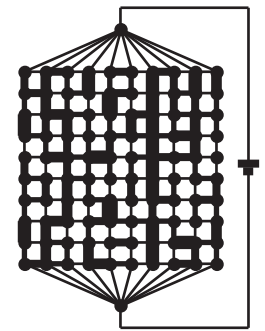
How does EPS affect fluid transport?



Krems, Eicken, Deming, PNAS 2011



RANDOM PIPE MODEL



- **Bimodal** lognormal distribution for brine inclusions
- Develop random pipe network model with bimodal distribution; Use numerical methods that can handle larger variances in sizes.
- Results predict observed drop in fluid permeability k .
- Rigorous bound on k for bimodal distribution of pore sizes

Steffen, Epshteyn, Zhu, Bowler, Deming, Golden
Multiscale Modeling and Simulation, 2018

Zhu, Jabini, Golden,
Eicken, Morris
Ann. Glac. 2006

How does the biology affect the physics?

Notices

of the American Mathematical Society

May 2009

Volume 56, Number 5

Climate Change and
the Mathematics of
Transport in Sea Ice

page 562

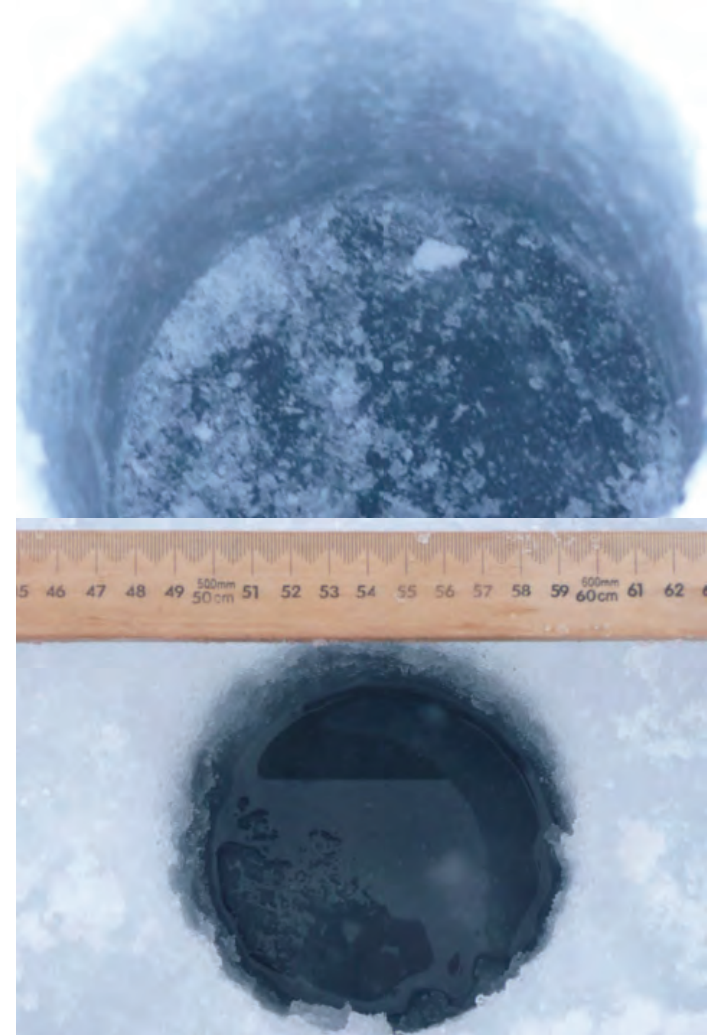
Mathematics and the
Internet: A Source of
Enormous Confusion
and Great Potential

page 586



photo by Jan Lieser

Real analysis in polar coordinates (see page 613)



**measuring
fluid permeability
of Antarctic sea ice**

SIPEX 2007

The Melt Pond Conundrum:

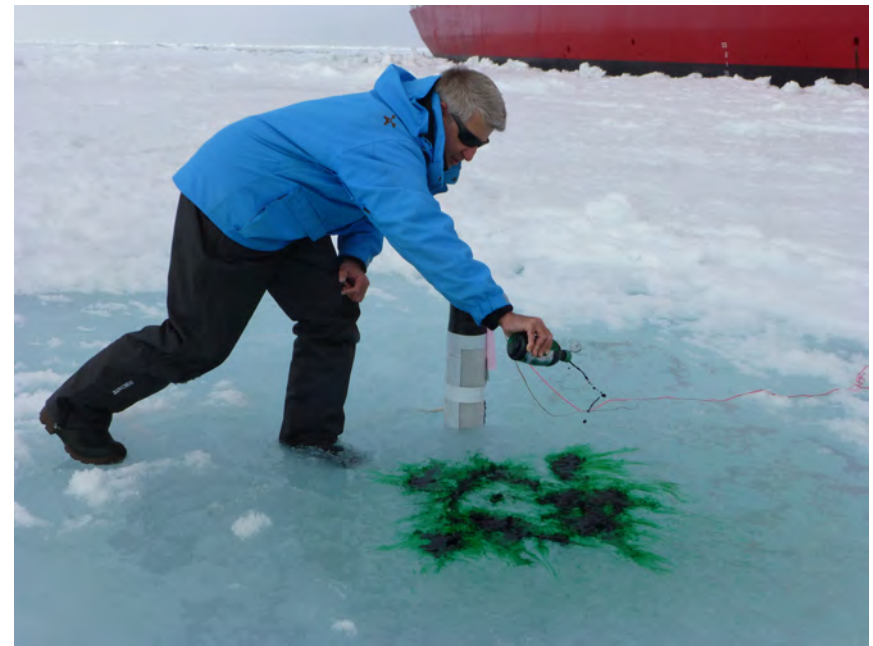
How can ponds form on top of sea ice that is highly permeable?

C. Polashenski, K. M. Golden, D. K. Perovich, E. Skyllingstad, A. Arnsten, C. Stwertka, N. Wright

Percolation Blockage: A Process that Enables Melt Pond Formation on First Year Arctic Sea Ice

J. Geophys. Res. Oceans 2017

*2014 Study of Under Ice Blooms in the Chuckchi Ecosystem (SUBICE)
aboard USCGC Healy*



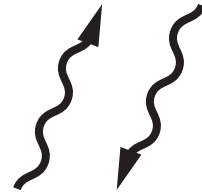
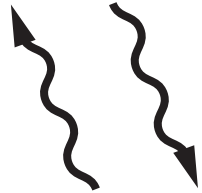
Remote sensing of sea ice

INVERSE PROBLEM

Recover sea ice properties from electromagnetic (EM) data

$$\epsilon^*$$

effective complex permittivity
(dielectric constant, conductivity)

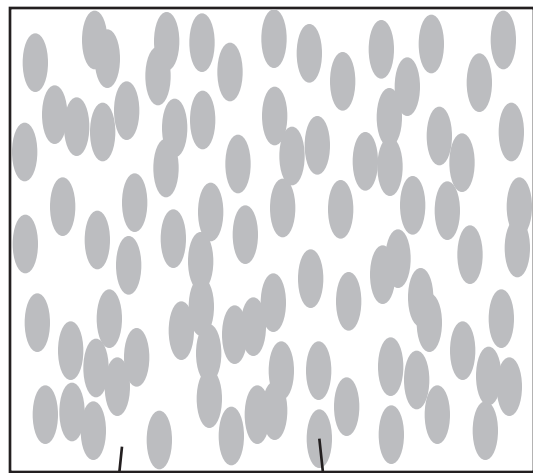


sea ice thickness
ice concentration



brine volume fraction
brine inclusion connectivity

Effective complex permittivity of a two phase composite in the quasistatic (long wavelength) limit



ϵ_1 ϵ_2



ϵ^*

$$D = \epsilon E$$

$$\nabla \cdot D = 0$$

$$\nabla \times E = 0$$

$$\langle D \rangle = \epsilon^* \langle E \rangle$$

p_1, p_2 = volume fractions of
the components

$$\epsilon^* = \epsilon^* \left(\frac{\epsilon_1}{\epsilon_2}, \text{ composite geometry} \right)$$

**What are the effective propagation characteristics
of an EM wave (radar, microwaves) in the medium?**

Analytic Continuation Method for Homogenization

Bergman (1978), Milton (1979), Golden and Papanicolaou (1983), Theory of Composites, Milton (2002)

Stieltjes integral representation for homogenized parameter

separates geometry from parameters

$$F(s) = 1 - \frac{\epsilon^*}{\epsilon_2} = \int_0^1 \frac{d\mu(z)}{s - z}$$

← geometry

← material parameters

$$s = \frac{1}{1 - \epsilon_1 / \epsilon_2}$$

μ

- spectral measure of self adjoint operator $\Gamma\chi$
- mass = p_1
- higher moments depend on n -point correlations

$$\Gamma = \nabla(-\Delta)^{-1}\nabla.$$

χ = characteristic function of the brine phase

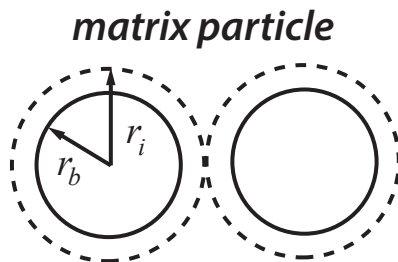
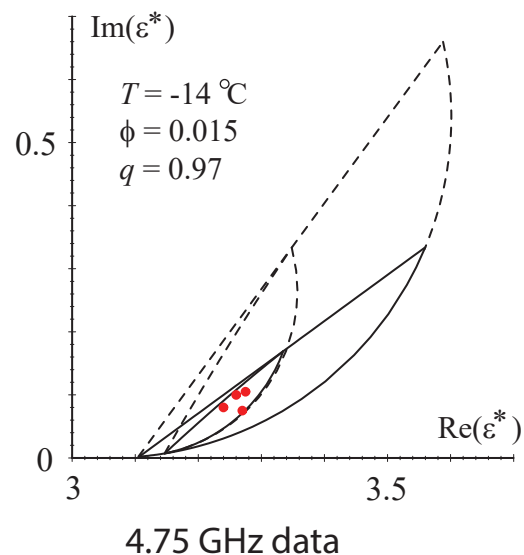
$$E = s (s + \Gamma\chi)^{-1} e_k$$

$\Gamma\chi$: microscale \rightarrow macroscale

$\Gamma\chi$ *links scales*

forward and inverse bounds on the complex permittivity of sea ice

forward bounds

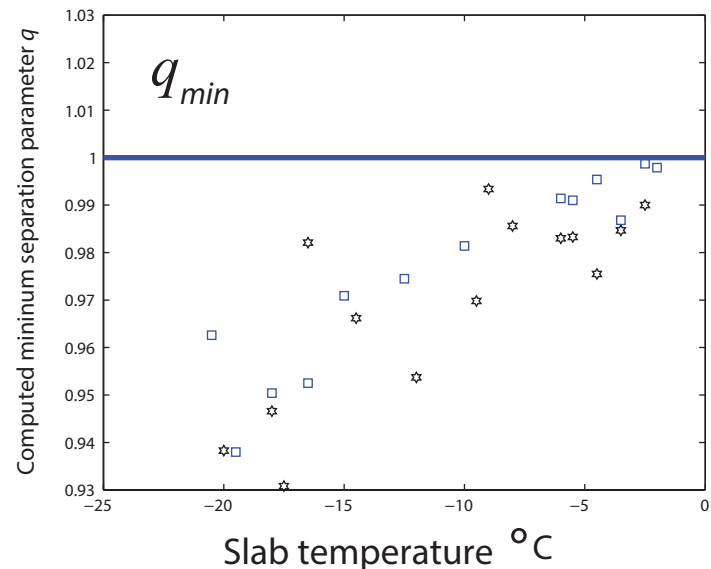


$$q = r_b / r_i$$

$$0 < q < 1$$

Golden 1995, 1997

inverse bounds



Inverse Homogenization

Cherkaev and Golden (1998), Day and Thorpe (1999), Cherkaev (2001), McPhedran, McKenzie, Milton (1982), *Theory of Composites*, Milton (2002)



inverse bounds and recovery of brine porosity

Gully, Backstrom, Eicken, Golden
Physica B, 2007

inversion for brine inclusion separations in sea ice from measurements of effective complex permittivity ϵ^*

rigorous inverse bound on spectral gap

construct algebraic curves which bound admissible region in (p,q) -space

Orum, Cherkaev, Golden
Proc. Roy. Soc. A, 2012

SEA ICE

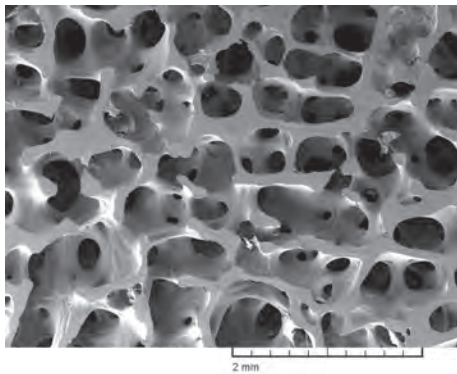


HUMAN BONE

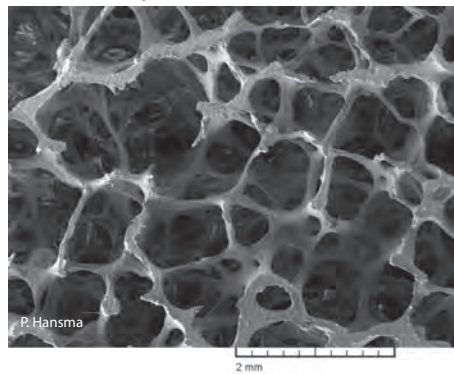


*spectral characterization
of porous microstructures
in human bone*

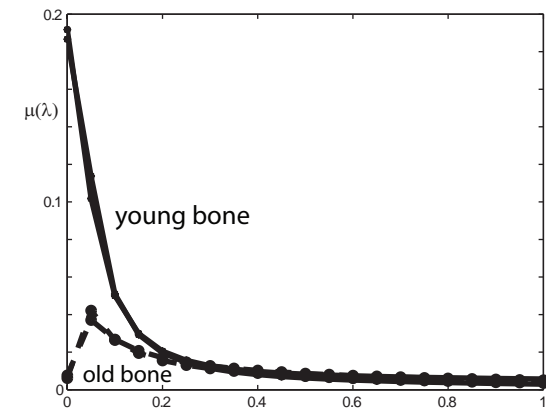
young healthy trabecular bone



old osteoporotic trabecular bone



reconstruct spectral measures
from complex permittivity data



use regularized inversion scheme

*apply spectral measure analysis of brine connectivity and
spectral inversion to electromagnetic monitoring of osteoporosis*

Golden, Murphy, Cherkaev, J. Biomechanics 2011

the math doesn't care if it's sea ice or bone!

direct calculation of spectral measures

Murphy, Hohenegger, Cherkaev, Golden, *Comm. Math. Sci.* 2015

- depends only on the composite geometry
- discretization of microstructural image gives binary network
- fundamental operator becomes a random matrix
- spectral measure computed from eigenvalues and eigenvectors

once we have the spectral measure μ it can be used in Stieltjes integrals for other transport coefficients:

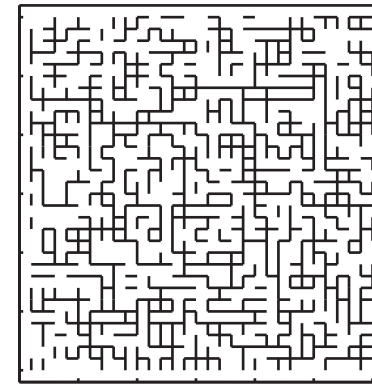
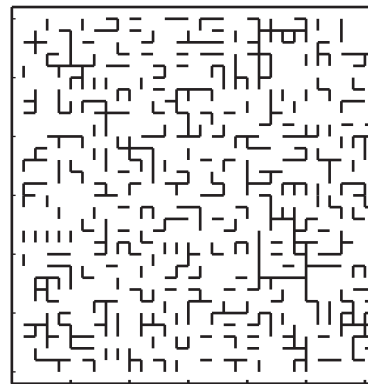
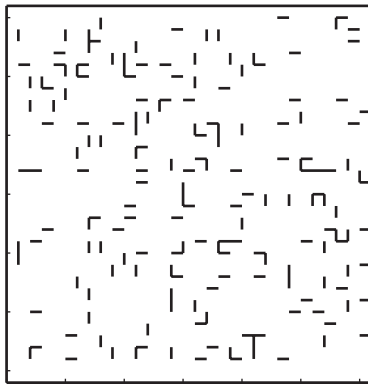
electrical and thermal conductivity, complex permittivity, magnetic permeability, diffusion, fluid flow properties

earlier studies of spectral measures

Day and Thorpe 1996

Helsing, McPhedran, Milton 2011

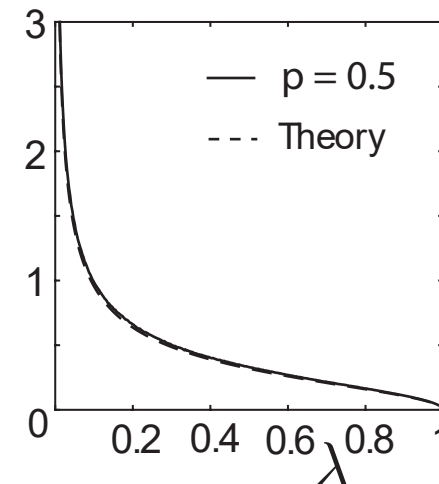
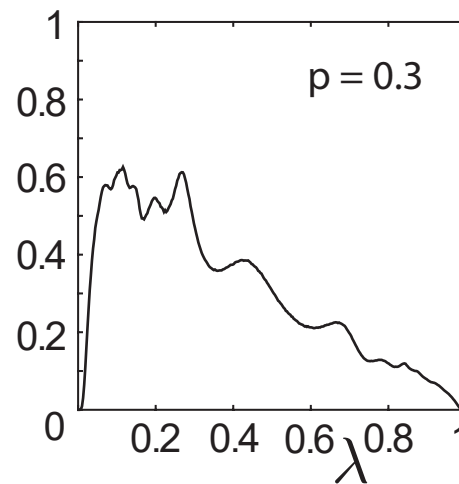
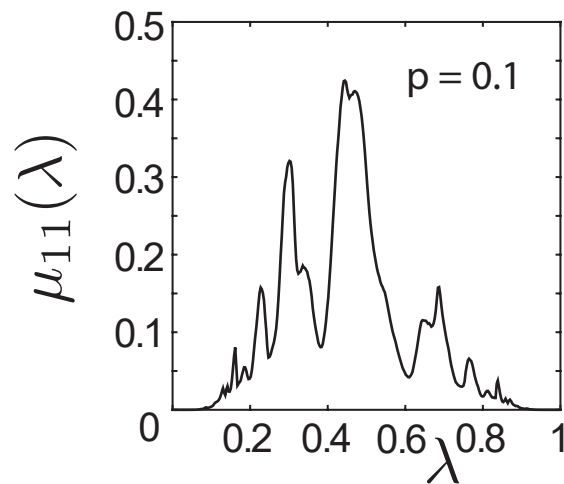
Spectral statistics for 2D random resistor network



Spectral Measures

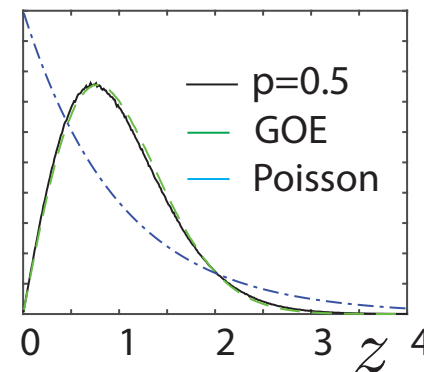
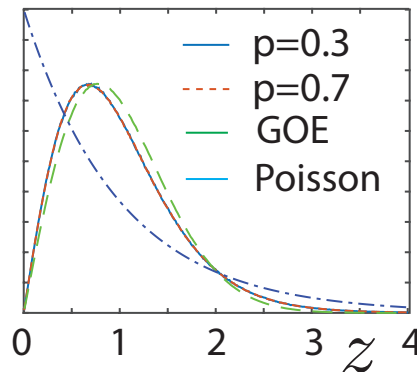
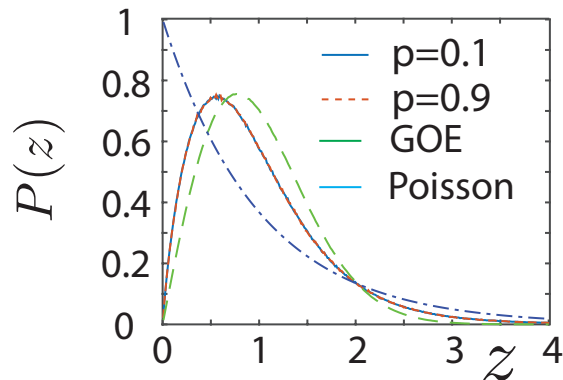
Murphy and Golden, *J. Math. Phys.*, 2012

Murphy et al. *Comm. Math. Sci.*, 2015



$p_c = 0.5$

Eigenvalue Spacing Distributions



Murphy,
Cherkaev,
Golden,
PRL, 2017

Eigenvalue Statistics of Random Matrix Theory

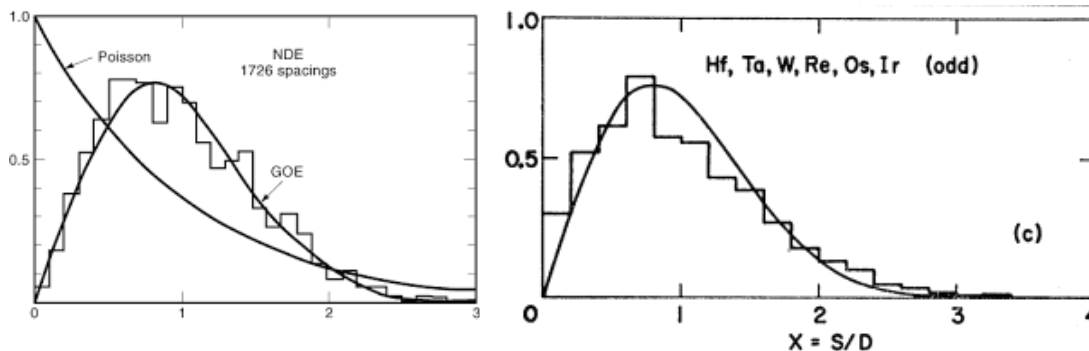
Wigner (1951) and Dyson (1953) first used random matrix theory (RMT) to describe quantized energy levels of heavy atomic nuclei.

$[\mathbf{N}]_{ij} \sim N(0,1), \quad \mathbf{A} = (\mathbf{N} + \mathbf{N}^T)/2 \quad \text{Gaussian orthogonal ensemble (GOE)}$

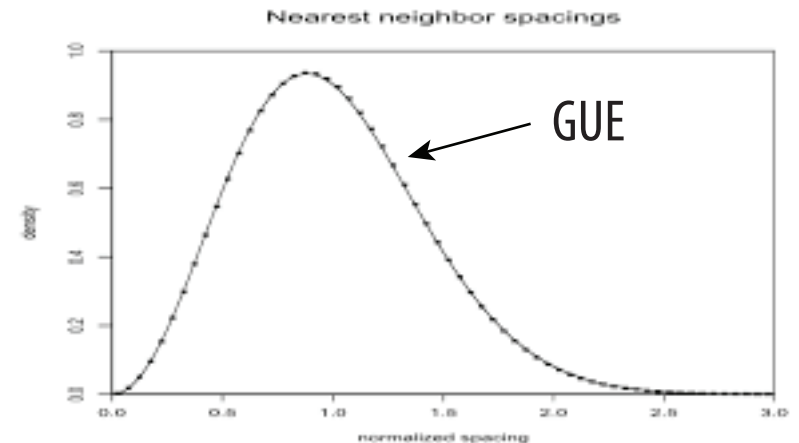
$[\mathbf{N}]_{ij} \sim N(0,1) + iN(0,1), \quad \mathbf{A} = (\mathbf{N} + \mathbf{N}^\dagger)/2 \quad \text{Gaussian unitary ensemble (GUE)}$

Short range and long range correlations of eigenvalues are measured by various eigenvalue statistics.

Spacing distributions of energy levels for heavy atomic nuclei



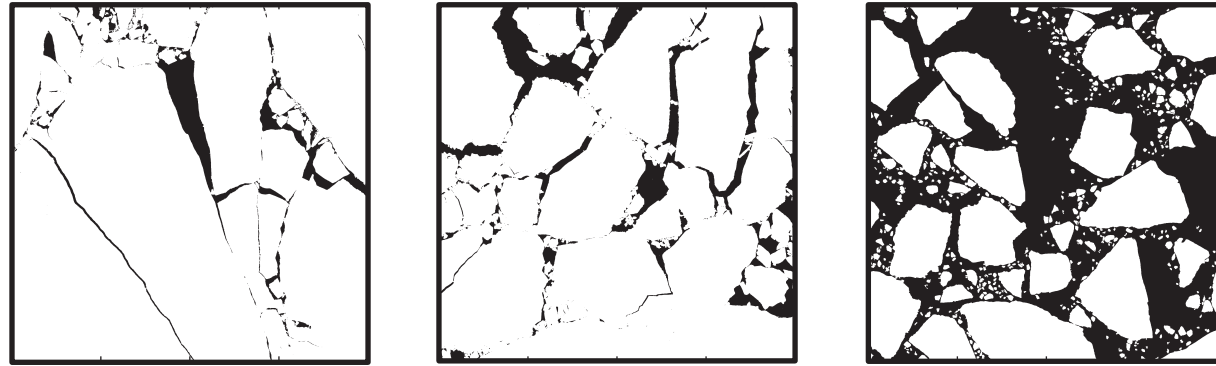
Spacing distributions of the first billion zeros of the Riemann zeta function



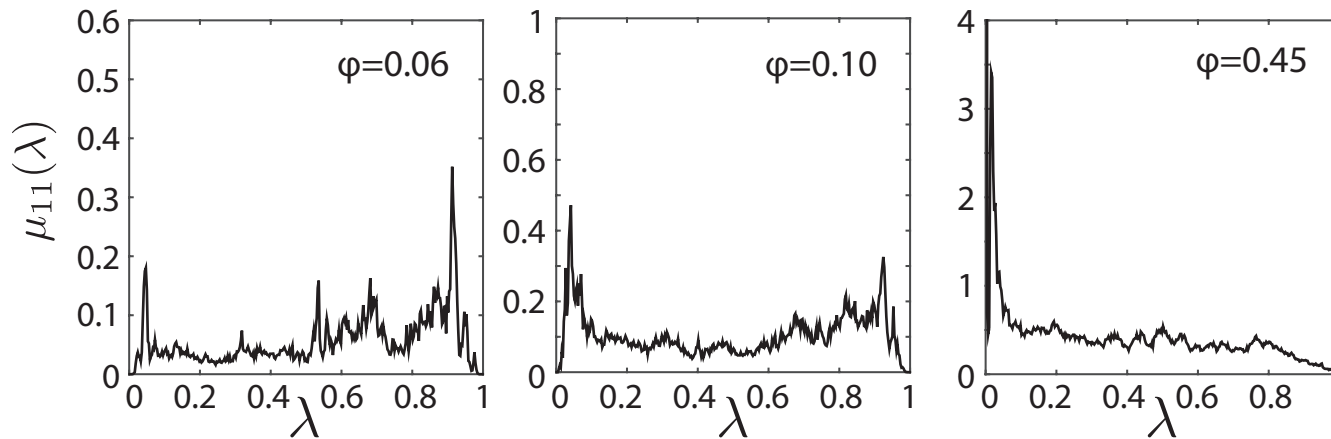
RMT used to characterize **disorder-driven transitions** in mesoscopic conductors, neural networks, random graph theory, etc.

Universal eigenvalue statistics arise in a broad range of “unrelated” problems!

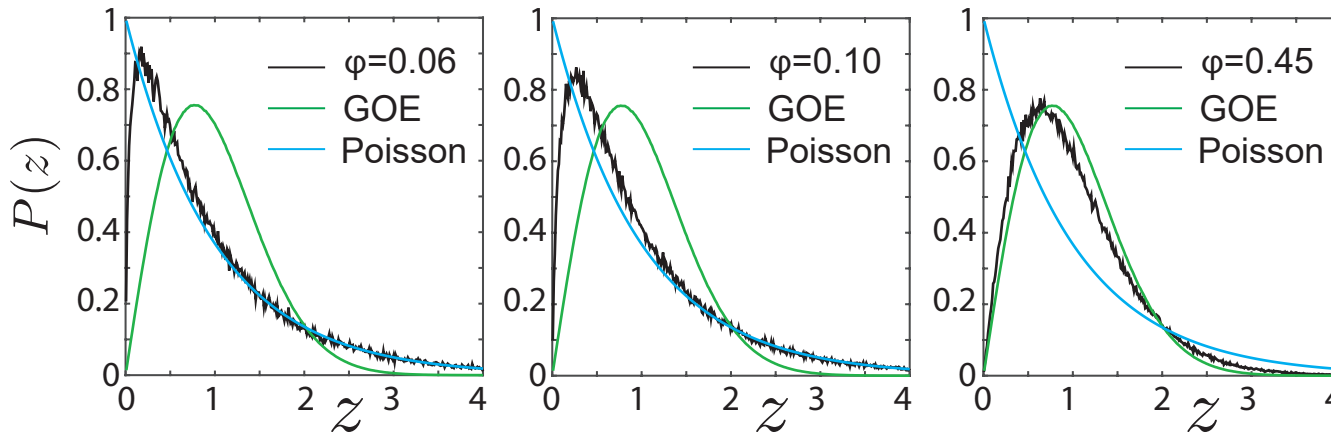
Spectral computations for sea ice floe configurations



spectral
measures



eigenvalue
spacing
distributions



uncorrelated

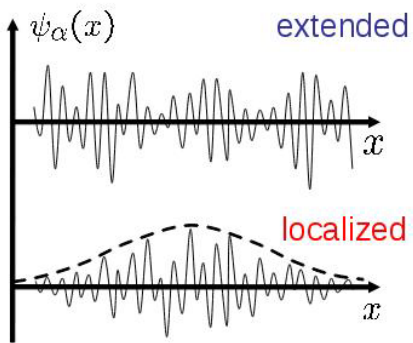


level repulsion

ANDERSON TRANSITION

Murphy, Cherkhev, Golden
Phys. Rev. Lett. 2017

**UNIVERSAL
Wigner-Dyson
distribution**



metal / insulator transition

localization

Anderson 1958
Mott 1949
Shklovshii et al 1993
Evangelou 1992

**Anderson transition in wave physics:
 quantum, optics, acoustics, water waves, ...**

from analysis of spectral measures for brine, melt ponds, ice floes

we find percolation-driven

Anderson transition for classical transport in composites

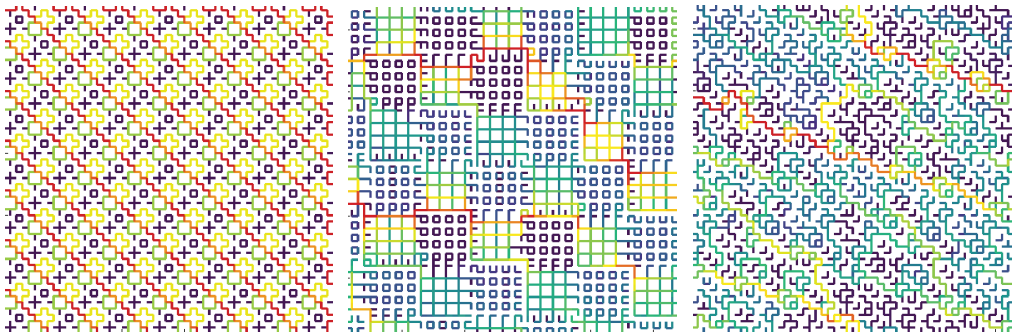
mobility edges, localization transition, universal spectral statistics

Murphy, Cherkhev, Golden Phys. Rev. Lett. 2017

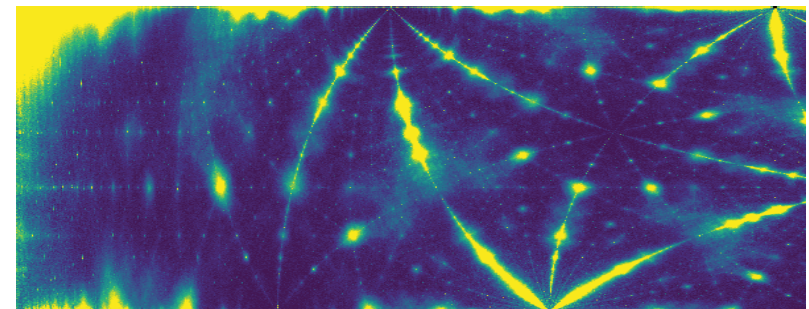
Order to disorder in quasiperiodic materials

Morison, Murphy, Cherkhev, Golden 2020

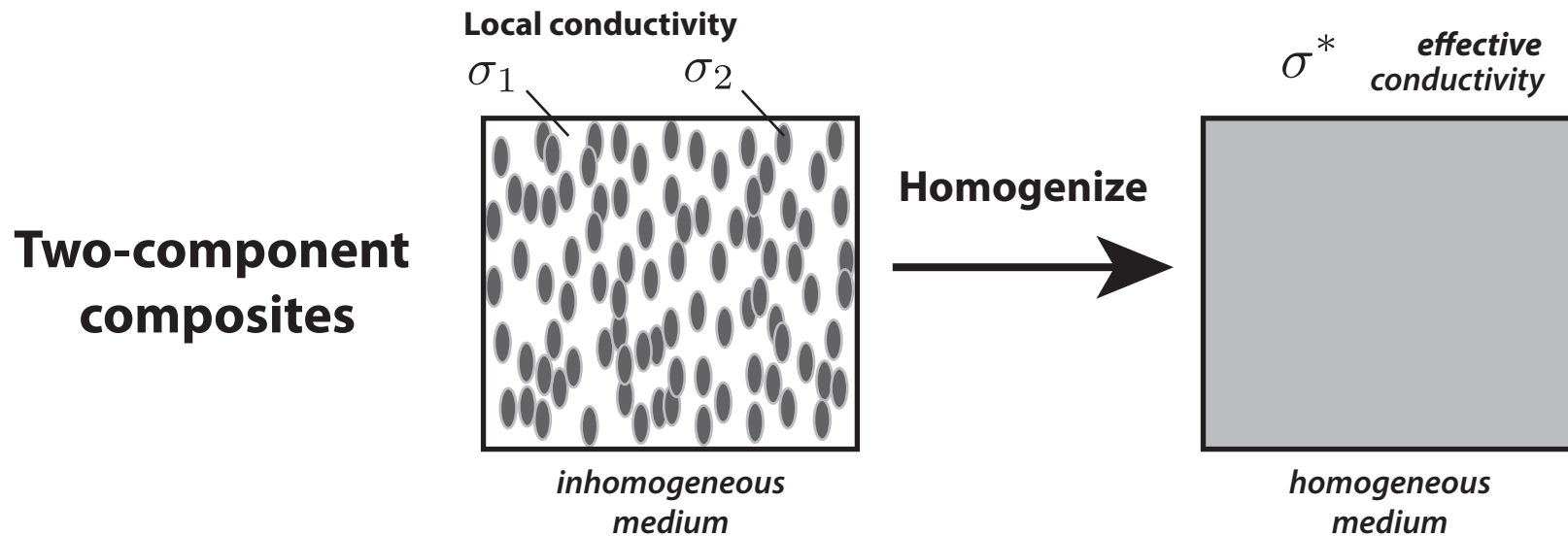
Parameterized Moiré Pattern Creates Tunable Microgeometry



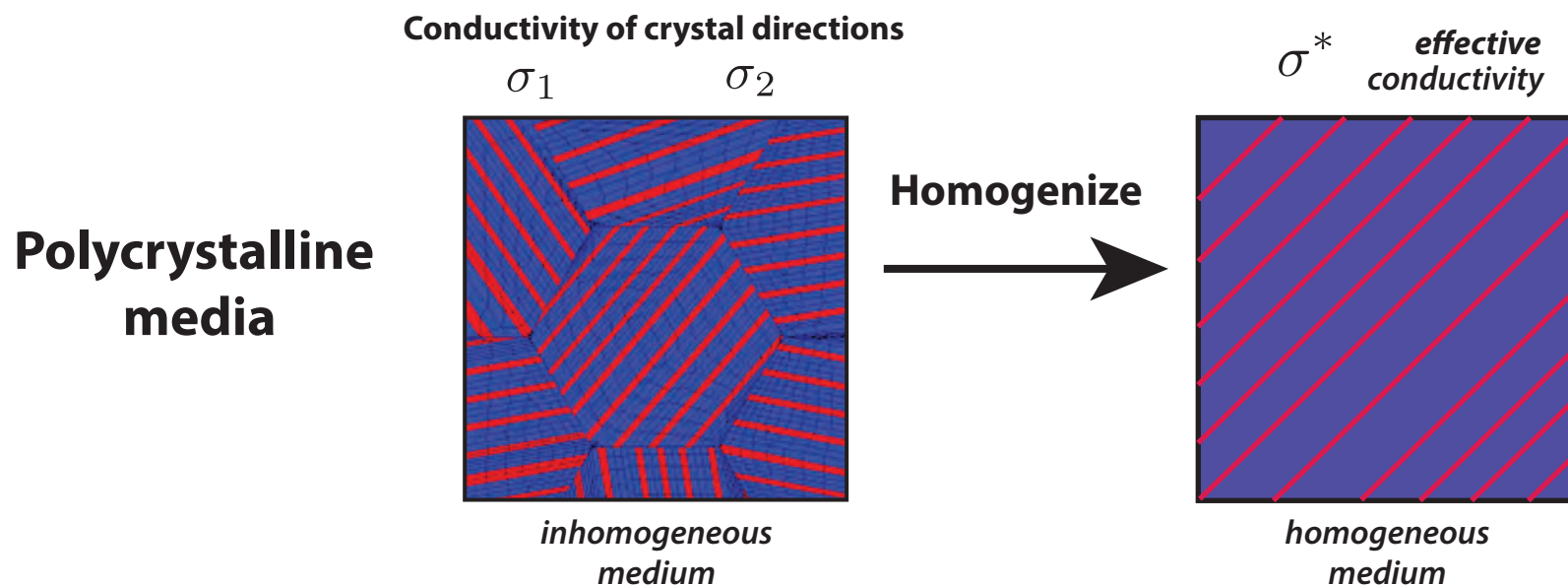
Anderson transition as QP is tuned



Homogenization for polycrystalline materials



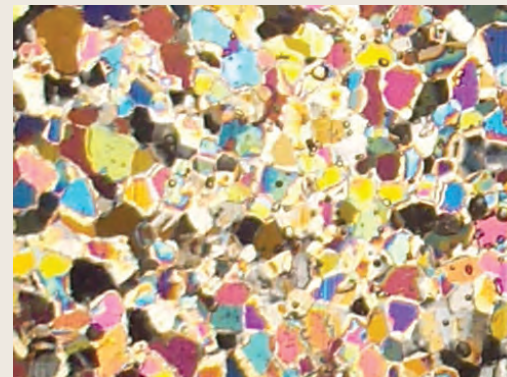
Find the homogeneous medium which behaves macroscopically the same as the inhomogeneous medium



Bounds on the complex permittivity of polycrystalline materials by analytic continuation

Adam Gully, Joyce Lin,
Elena Cherkaev, Ken Golden

- **Stieltjes integral representation for effective complex permittivity**
Milton (1981, 2002), Barabash and Stroud (1999), ...
- **Forward and inverse bounds**
orientation statistics
- **Applied to sea ice using two-scale homogenization**
- **Inverse bounds give method for distinguishing ice types using remote sensing techniques**



ISSN 1364-5021 | Volume 471 | Issue 2174 | 8 February 2015

PROCEEDINGS A

350 YEARS
OF SCIENTIFIC
PUBLISHING

An invited review commemorating 350 years of scientific publishing at the Royal Society

A method to distinguish between different types of sea ice using remote sensing techniques

A computer model to determine how a human should walk so as to expend the least energy



THE
ROYAL
SOCIETY
PUBLISHING

Proc. R. Soc. A | Volume 471 | Issue 2174 | 8 February 2015

higher threshold for fluid flow in granular sea ice

microscale details impact “mesoscale” processes

nutrient fluxes for microbes
melt pond drainage
snow-ice formation

columnar

granular

5%



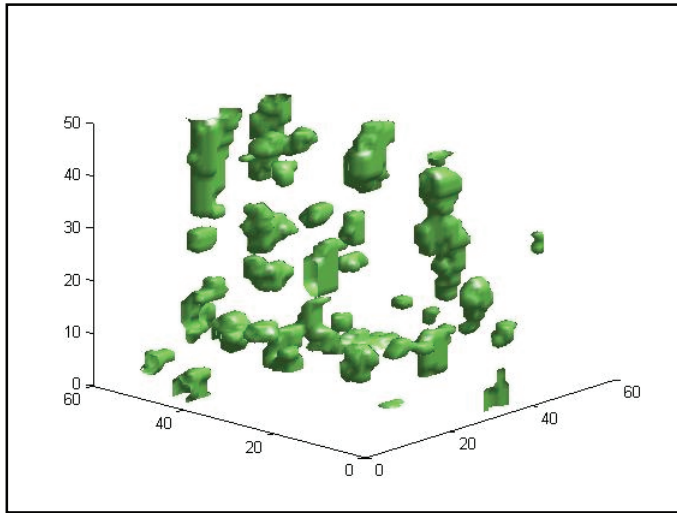
10%



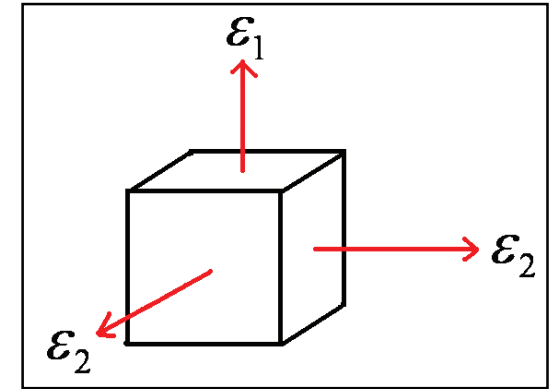
Golden, Sampson, Gully, Lubbers, Tison 2020

electromagnetically distinguishing ice types
Kitsel Lusted, Elena Cherkaev, Ken Golden

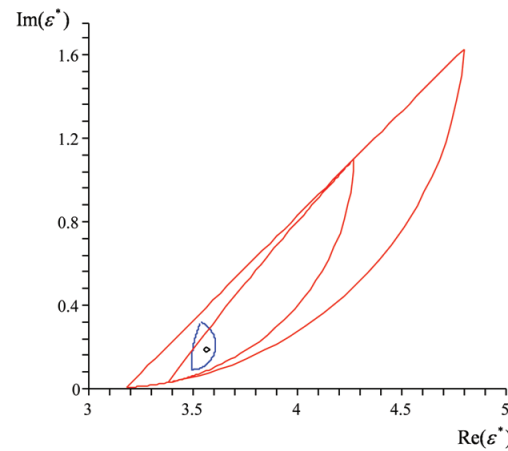
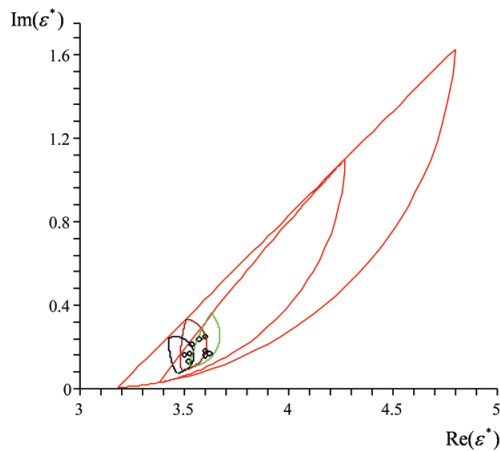
two scale homogenization for polycrystalline sea ice



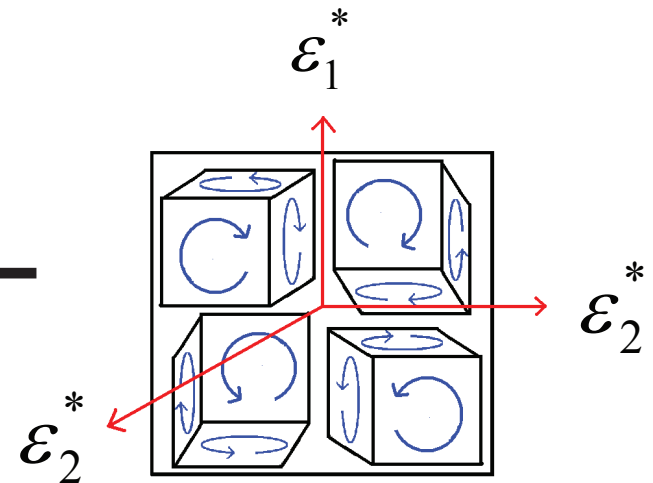
numerical homogenization
for single crystal



analytic continuation
for polycrystals



bounds



Rigorous bounds on the complex permittivity tensor of sea ice with polycrystalline anisotropy within the horizontal plane

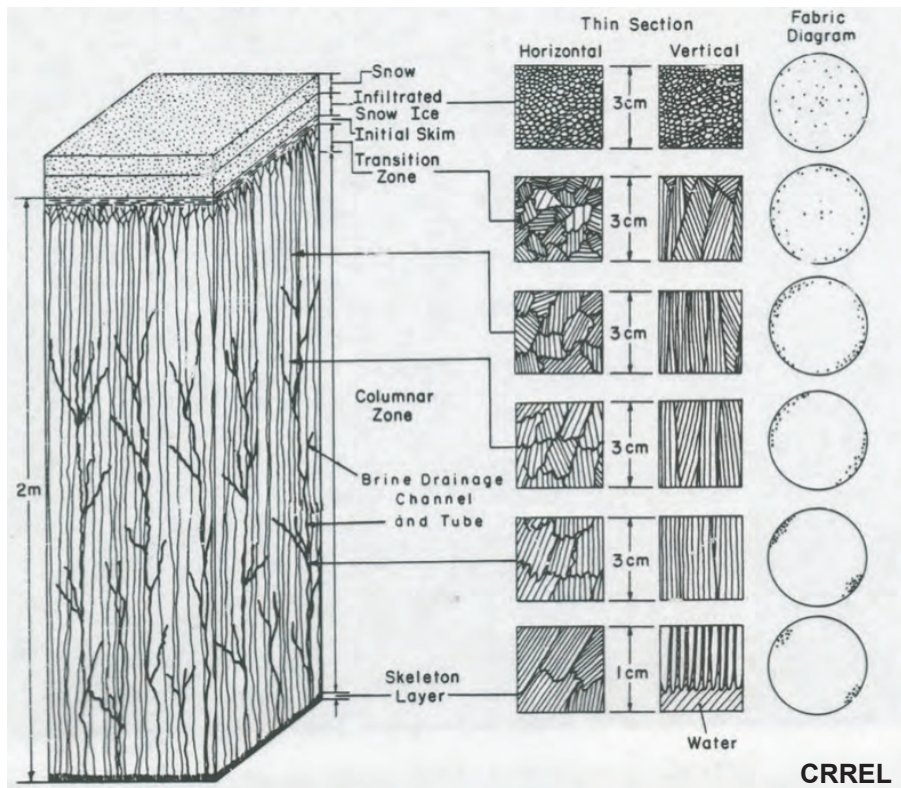
McKenzie McLean, Elena Cherkaev, Ken Golden 2020

motivated by

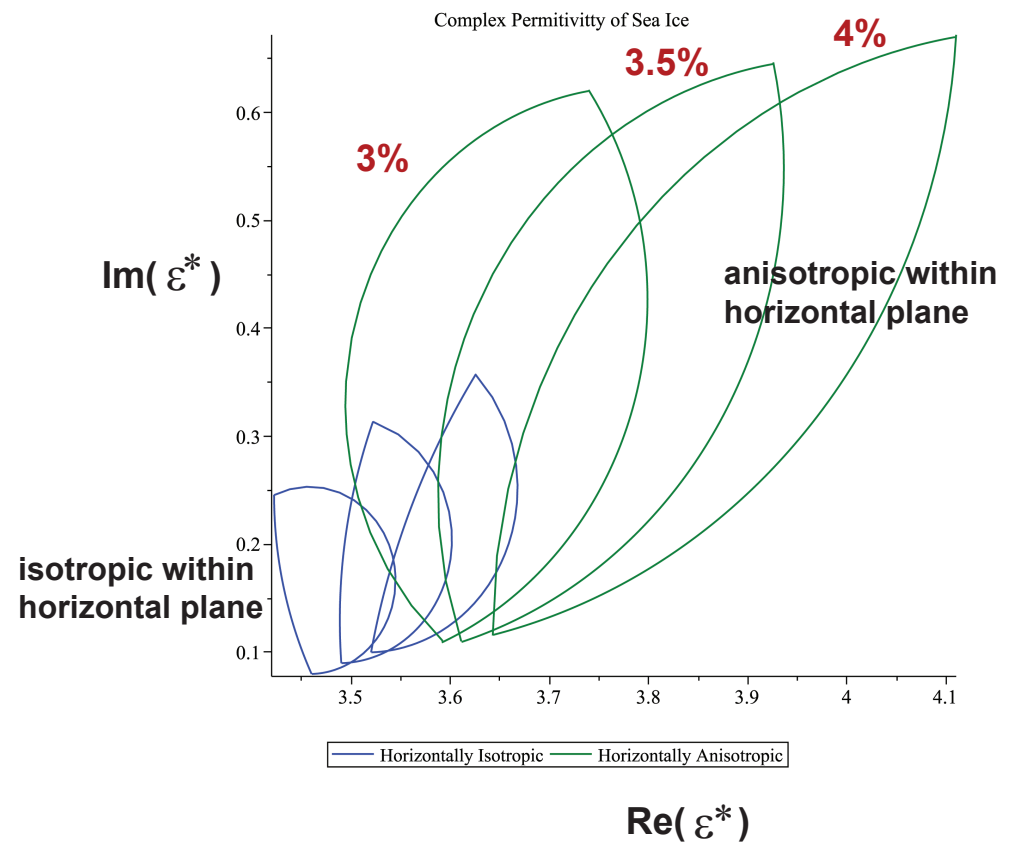
Weeks and Gow, *JGR* 1979: c-axis alignment in Arctic fast ice off Barrow

Golden and Ackley, *JGR* 1981: radar propagation model in aligned sea ice

input: orientation statistics



output: bounds



mesoscale

wave propagation in the marginal ice zone

Stieltjes integral representation
bounds on effective viscoelastic parameters

Sampson, Murphy, Cherkaev, Golden 2020

long wavelength

$$\langle \sigma_{ij} \rangle = C_{ijkl}^* \langle \epsilon_{kl} \rangle$$

ϵ_0 avg strain

$$C_{ijkl}^* = v^* \left(\delta_{ik} \delta_{jl} + \delta_{il} \delta_{jk} - \frac{2}{3} \delta_{ij} \delta_{kl} \right) = v^* \lambda_s$$

$$F(s) = 1 - \frac{v^*}{v_2} \quad s = \frac{1}{1 - \frac{v_1}{v_2}}$$

$$F(s) = \|\epsilon_0\|^{-2} \int_{\Sigma} \frac{d\mu(\lambda)}{s - \lambda}$$

resolvent for strain field

$$\epsilon = \left(1 - \frac{1}{s} \Gamma \chi \right)^{-1} \epsilon_0$$

$$\Gamma = \nabla^s (\nabla \cdot \nabla^s)^{-1} \nabla \cdot$$

local

$$\sigma_{ij} = C_{ijkl} \epsilon_{kl}$$

quasistatic

$$\nabla \cdot \sigma = 0$$



bounds on the effective complex viscoelasticity

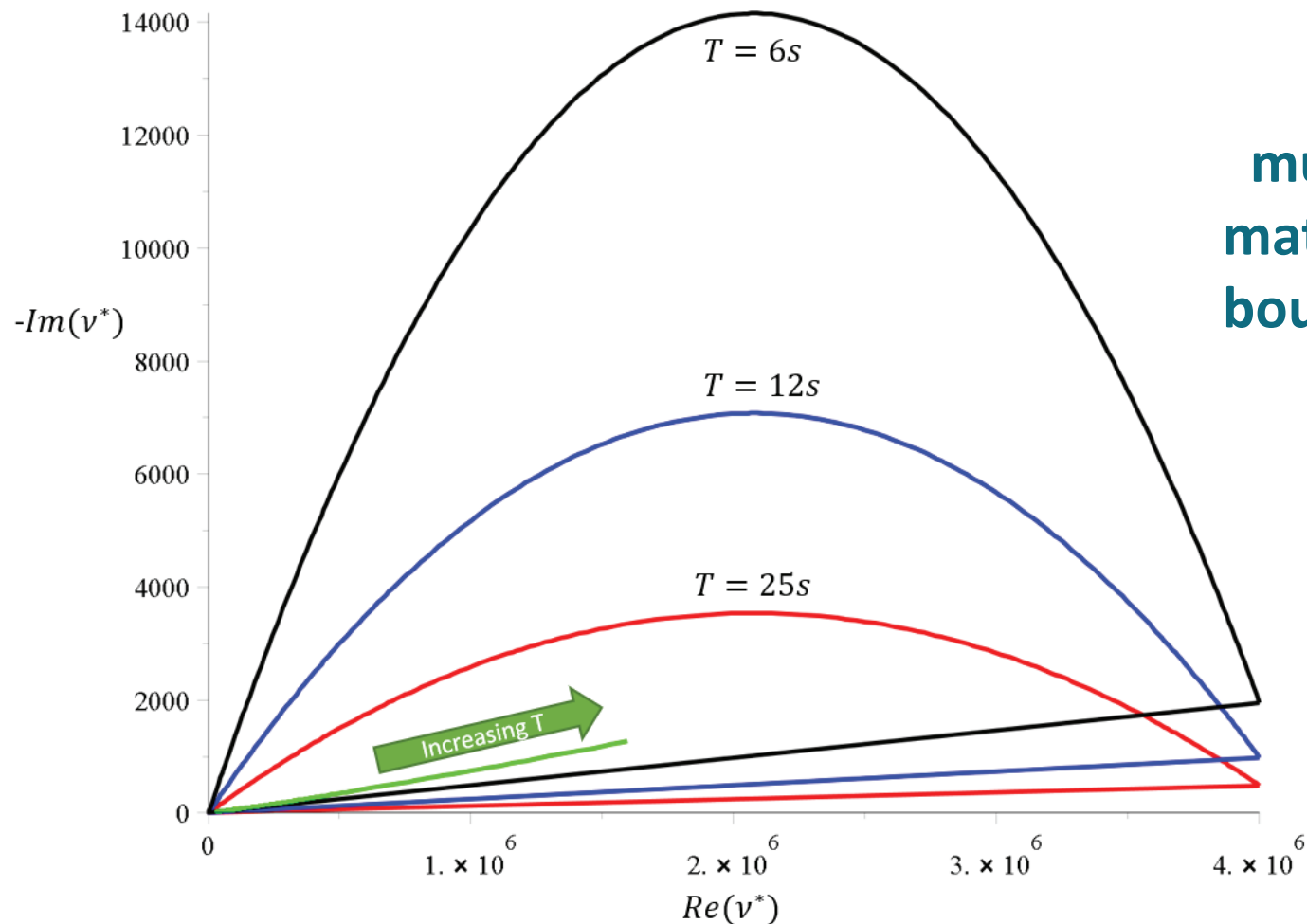
complex elementary bounds
(fixed area fraction of floes)

$$V_1 = 10^7 + i4875$$

pancake ice

$$V_2 = 5 + i0.0975$$

slush / frazil

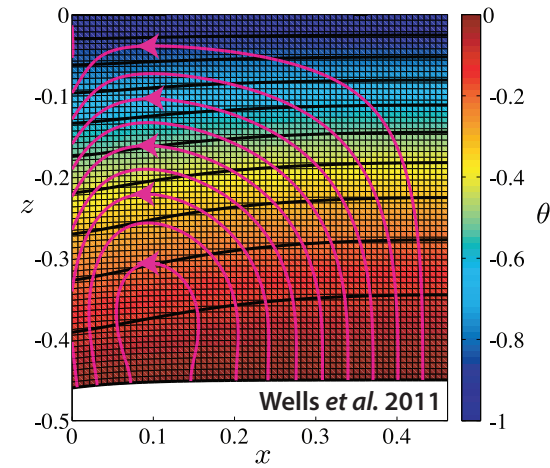
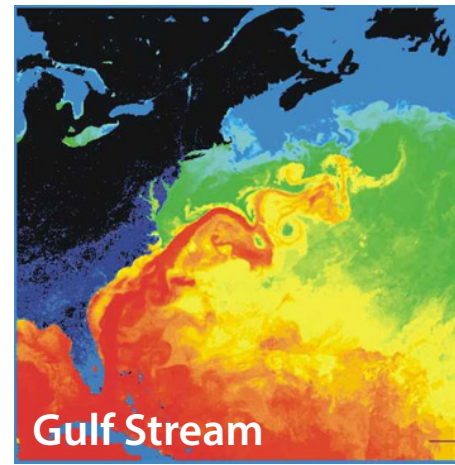


+
much tighter
matrix particle
bounds + data

advection enhanced diffusion

effective diffusivity

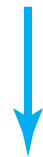
- nutrient and salt transport in sea ice
- heat transport in sea ice with convection
- sea ice floes in winds and ocean currents
- tracers, buoys diffusing in ocean eddies
- diffusion of pollutants in atmosphere



advection diffusion equation with a velocity field \vec{u}

$$\frac{\partial T}{\partial t} + \vec{u} \cdot \vec{\nabla} T = \kappa_0 \Delta T$$

$$\vec{\nabla} \cdot \vec{u} = 0$$



homogenize

$$\frac{\partial \bar{T}}{\partial t} = \kappa^* \Delta \bar{T}$$

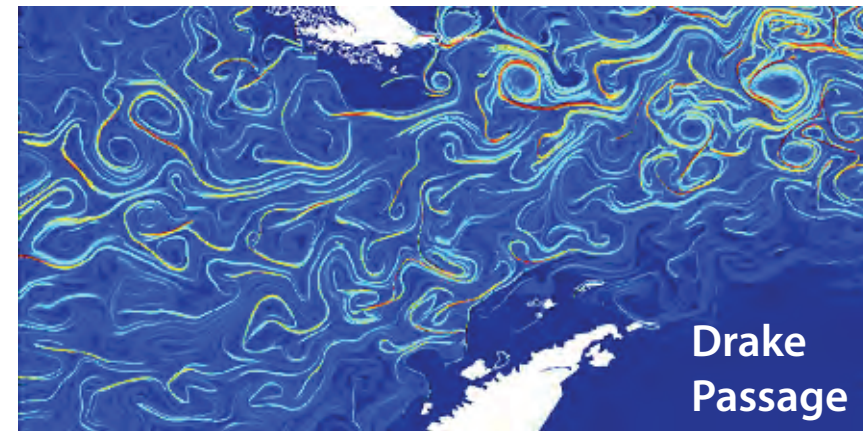
κ^* effective diffusivity

Stieltjes integral for κ^* with spectral measure

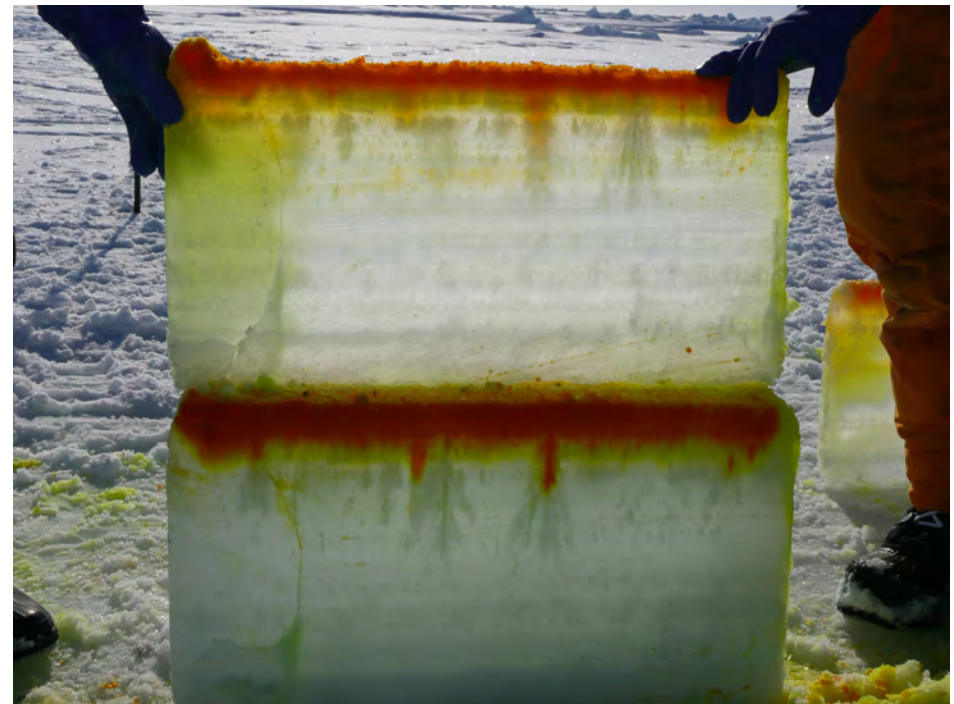
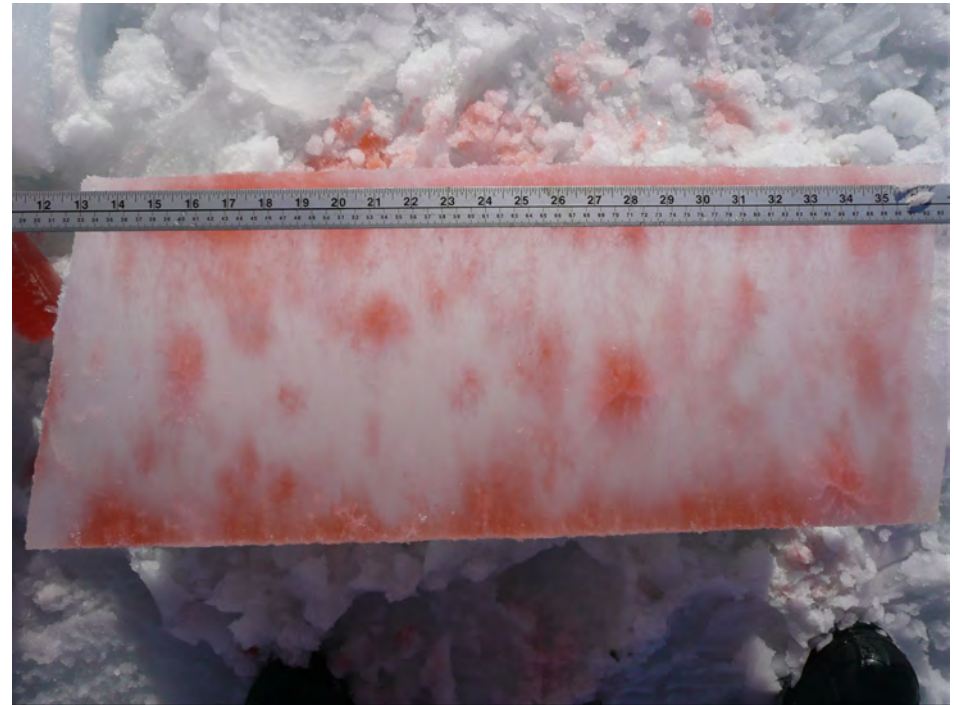
Avellaneda and Majda, PRL 89, CMP 91

Murphy, Cherkaev, Xin, Zhu, Golden, Ann. Math. Sci. Appl. 2017

Murphy, Cherkaev, Zhu, Xin, Golden, J. Math. Phys. 2020



tracers flowing through inverted sea ice blocks



Stieltjes Integral Representation for Advection Diffusion

Murphy, Cherkaev, Zhu, Xin, Golden, *J. Math. Phys.* 2020

$$\kappa^* = \kappa \left(1 + \int_{-\infty}^{\infty} \frac{d\mu(\tau)}{\kappa^2 + \tau^2} \right), \quad F(\kappa) = \int_{-\infty}^{\infty} \frac{d\mu(\tau)}{\kappa^2 + \tau^2}$$

- μ is a positive definite measure corresponding to the spectral resolution of the self-adjoint operator $i\Gamma H\Gamma$
- $H =$ stream matrix , $\kappa =$ local diffusivity
- $\Gamma := -\nabla(-\Delta)^{-1}\nabla\cdot$, Δ is the Laplace operator
- $i\Gamma H\Gamma$ is bounded for time independent flows
- $F(\kappa)$ is analytic off the spectral interval in the κ -plane

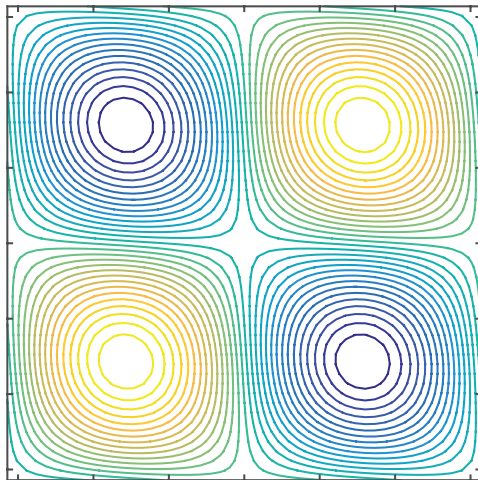
rigorous framework for numerical computations of spectral measures and effective diffusivity for model flows

new integral representations, theory of moment calculations

separation of material properties and flow field

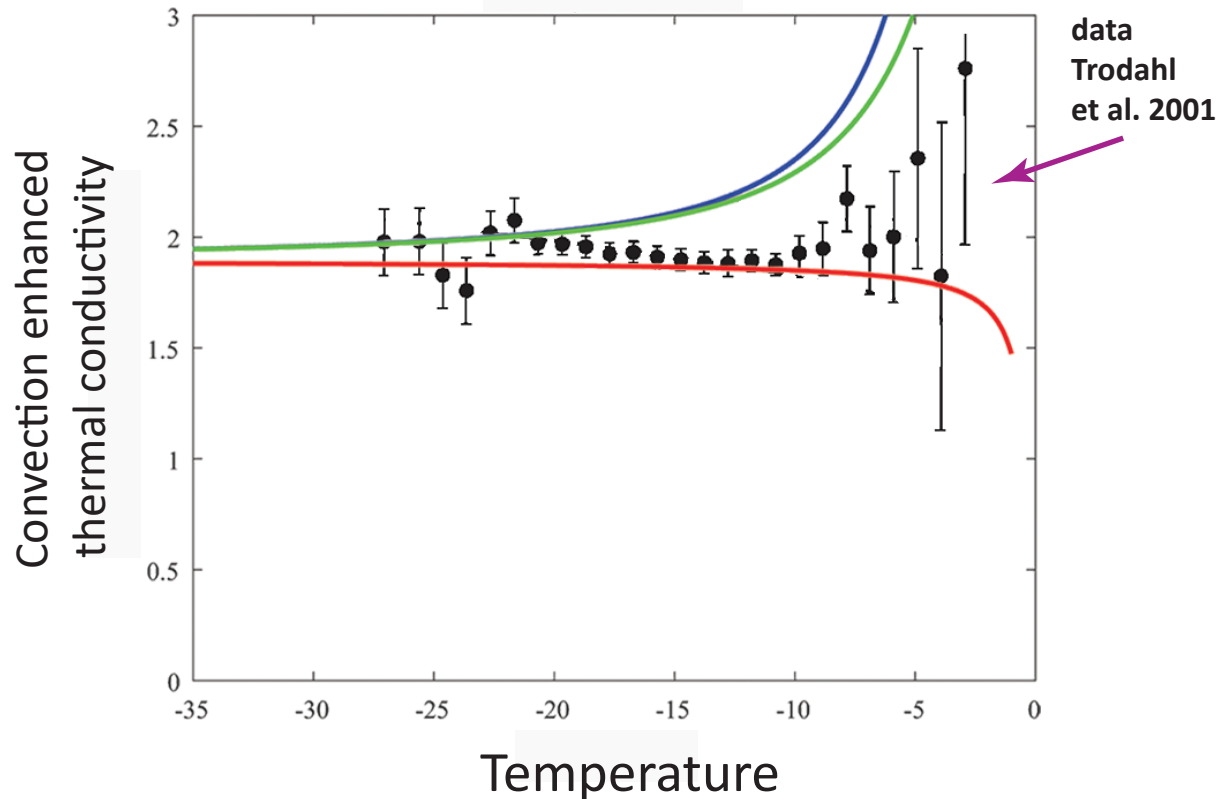
Rigorous bounds on convection enhanced thermal conductivity of sea ice

Kraitzman, Hardenbrook, Murphy, Zhu, Cherkaev, Strong, Golden 2020



cat's eye flow model for brine convection cells

similar bounds for shear flows



rigorous Padé bounds from Stieltjes integral + analytical calculations of moments of measure

rigorous bounds assuming information on flow field INSIDE inclusions

melt pond formation and albedo evolution:

- *major drivers in polar climate*
- *key challenge for global climate models*

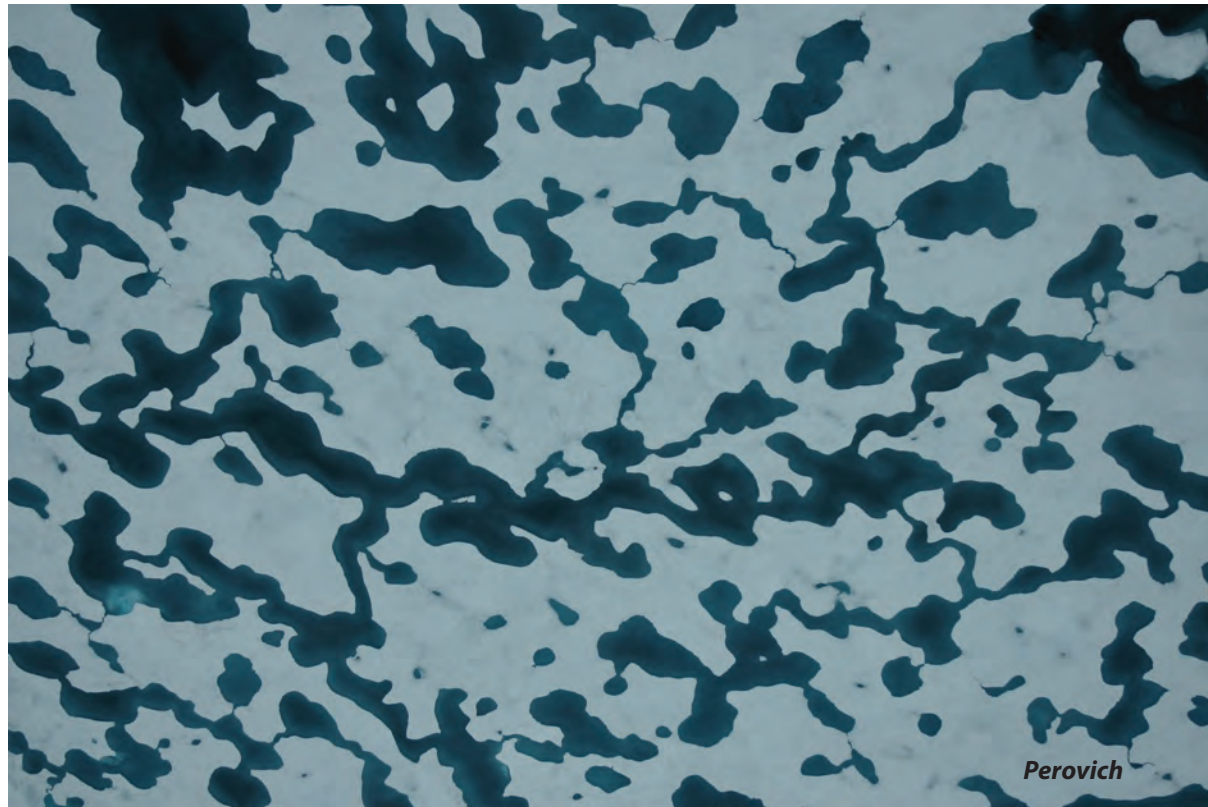
numerical models of melt pond evolution, including topography, drainage (permeability), etc.

Lüthje, Feltham,
Taylor, Worster 2006

Flocco, Feltham 2007

Skyllingstad, Paulson,
Perovich 2009

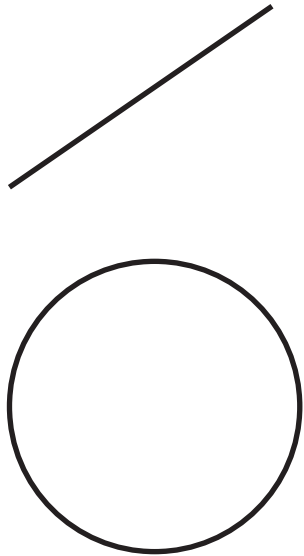
Flocco, Feltham,
Hunke 2012



Are there universal features of the evolution similar to phase transitions in statistical physics?

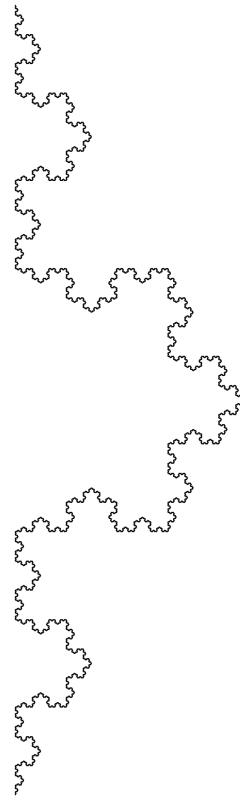
fractal curves in the plane

they wiggle so much that their dimension is >1



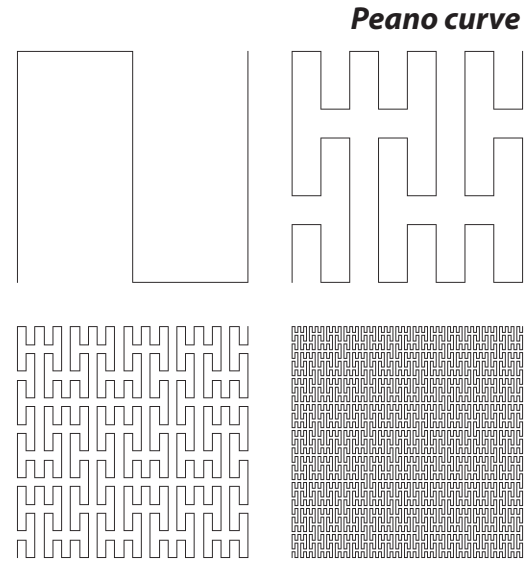
simple curves

$D = 1$



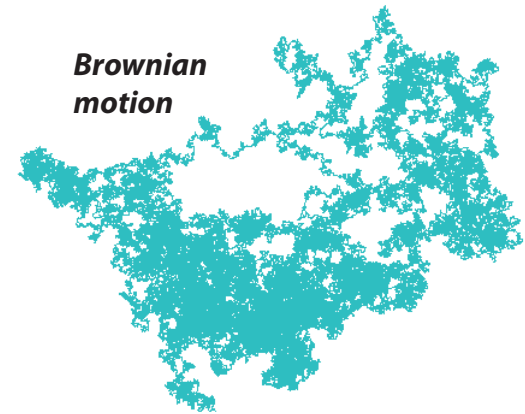
Koch snowflake

$D = 1.26$



Peano curve

Brownian motion



space filling curves

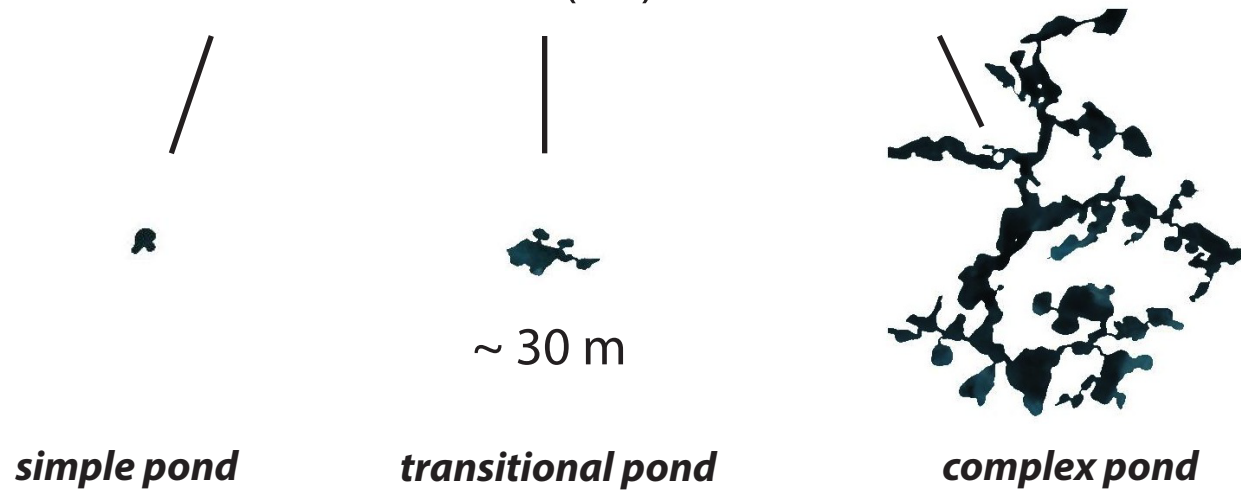
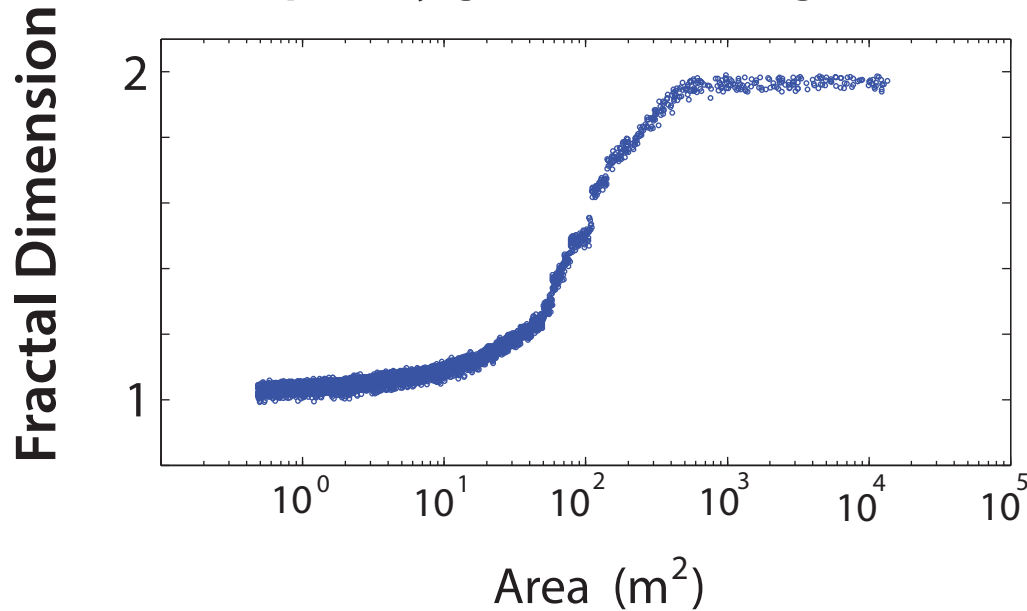
$D = 2$

Transition in the fractal geometry of Arctic melt ponds

Christel Hohenegger, Bacim Alali, Kyle Steffen, Don Perovich, Ken Golden

The Cryosphere, 2012

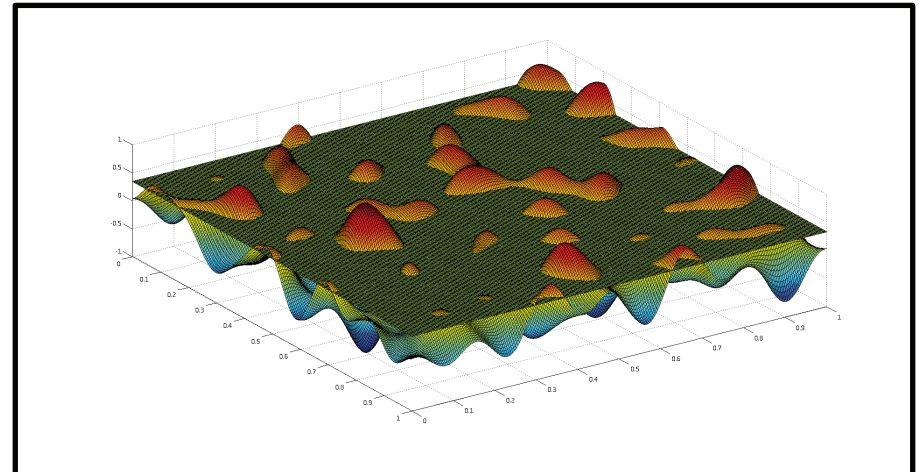
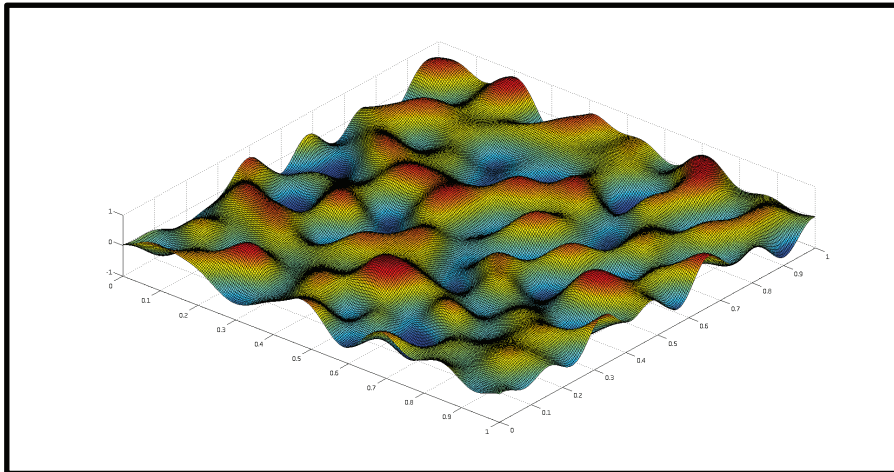
complexity grows with length scale



Continuum percolation model for melt pond evolution

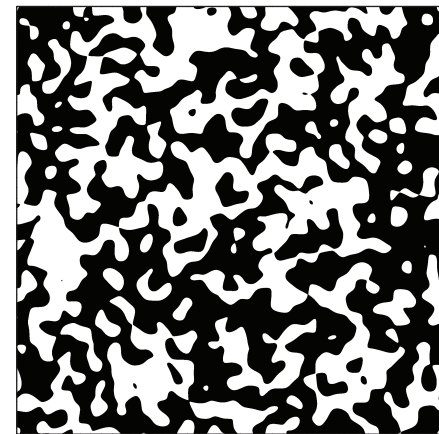
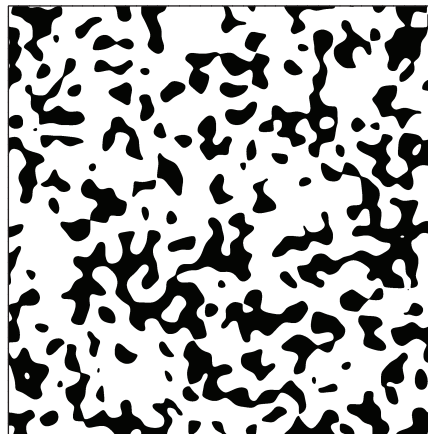
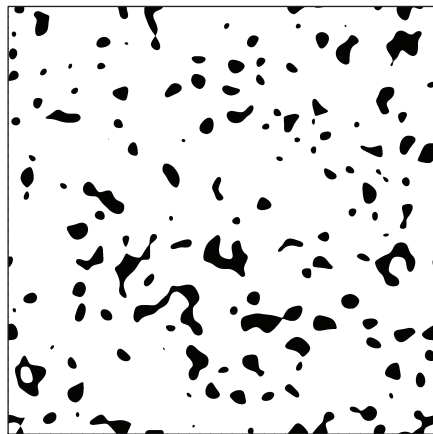
level sets of random surfaces

Brady Bowen, Court Strong, Ken Golden, J. Fractal Geometry 2018



random Fourier series representation of surface topography

intersections of a plane with the surface define melt ponds

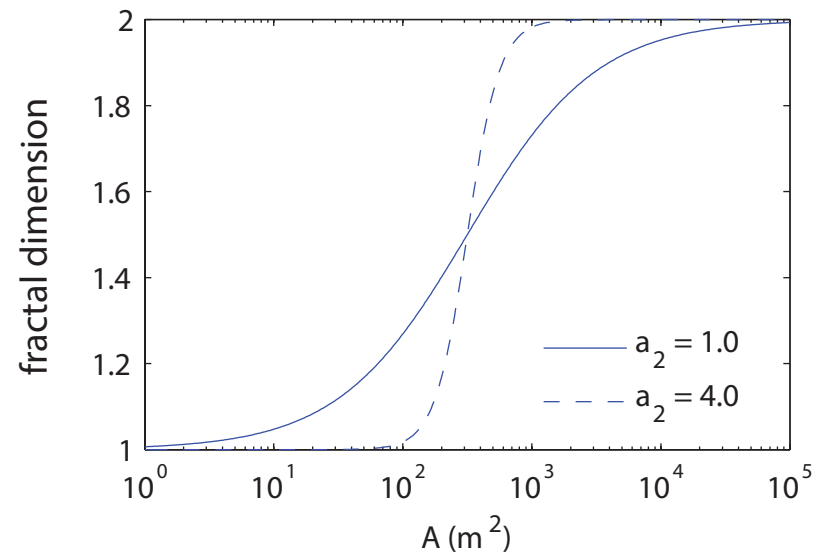
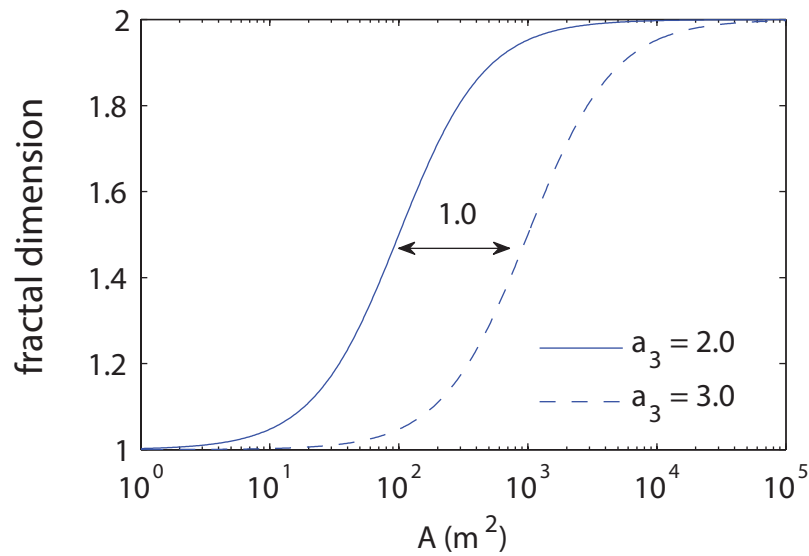


electronic transport in disordered media

diffusion in turbulent plasmas

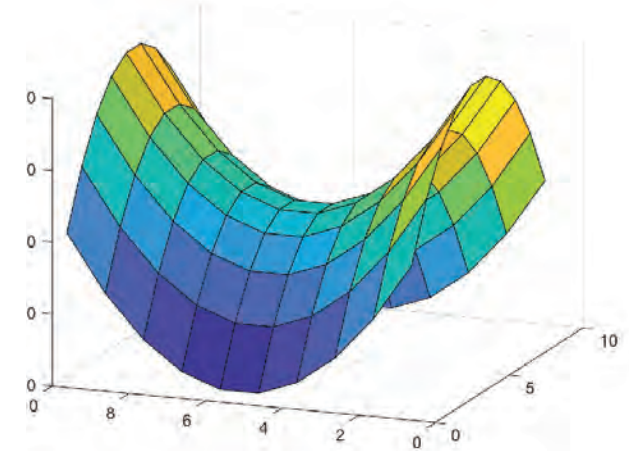
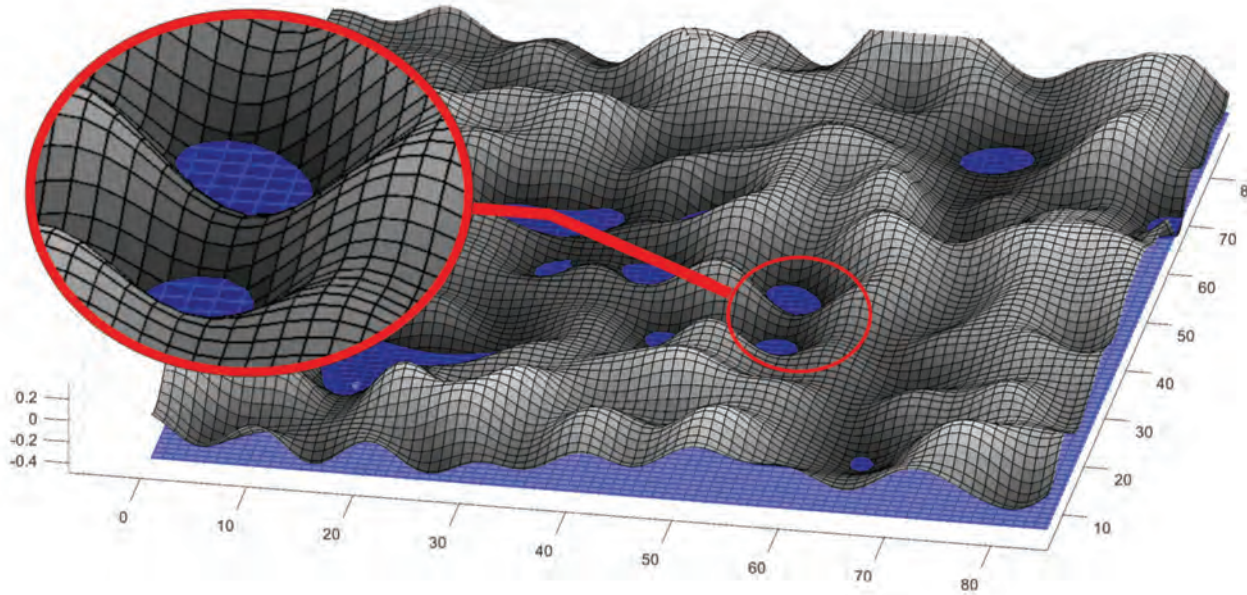
Isichenko, Rev. Mod. Phys., 1992

fractal dimension curves depend on statistical parameters defining random surface

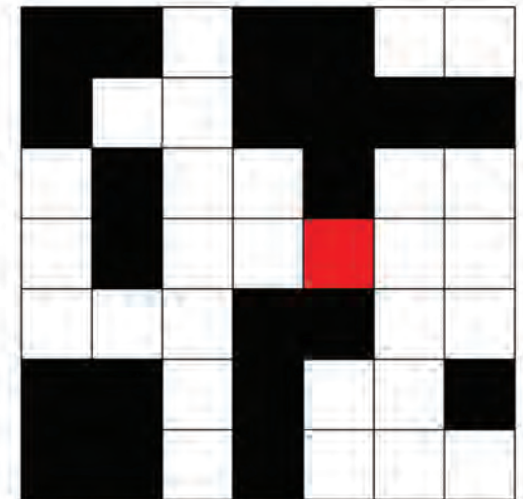


Saddle Points: The Key to Melt Pond Evolution

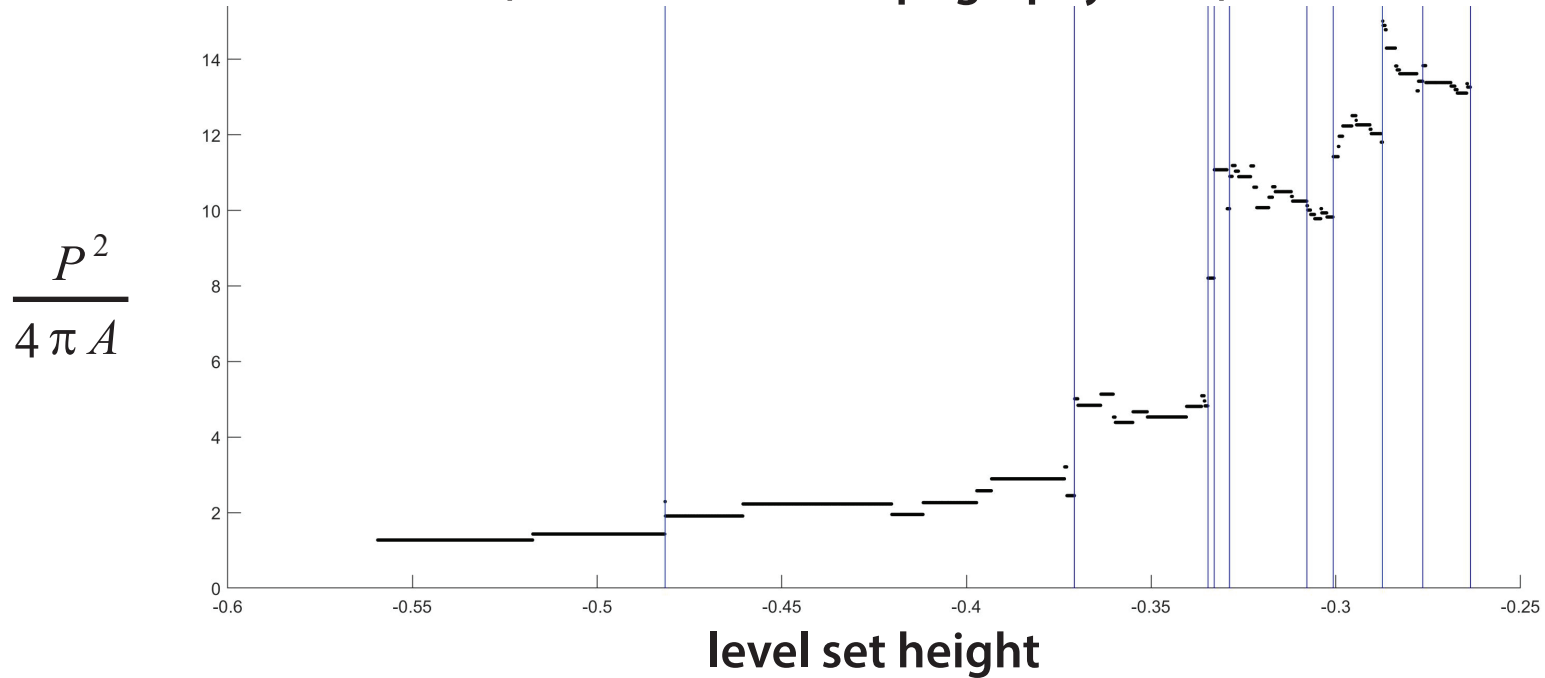
Ryleigh Moore, Jacob Jones, Dane Gollero, Court Strong, Ken Golden 2020



- Ponds connect through saddle points (Morse Theory).
- Red bond bond in percolation theory ~ saddle point.



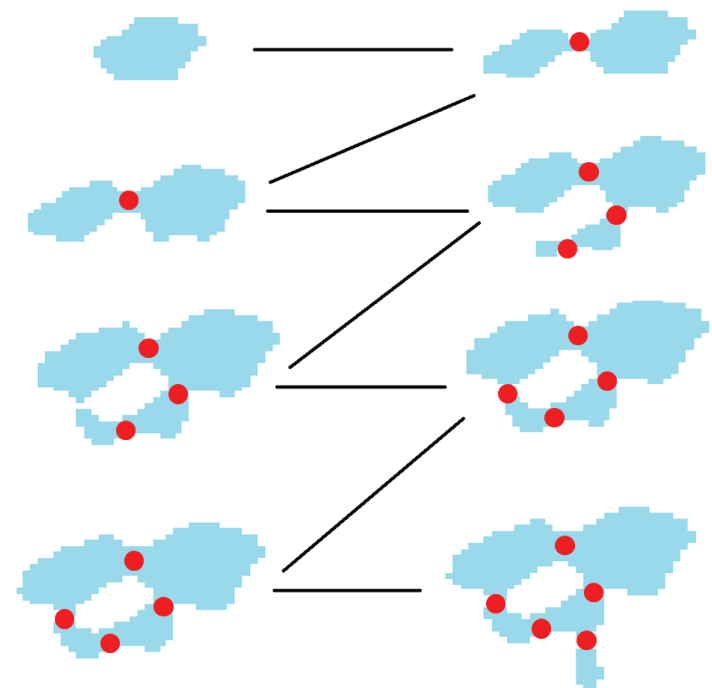
Evolution of Isoperimetric Quotient with Melt Pond Growth (from real snow topography data)



In the graph, we follow a single pond's growth. The vertical lines denote when the pond goes through a saddle point.

We see that large jumps in fractal dimension occur through saddle points.

pond coalescence and thickening





Ryleigh Moore, University of Utah

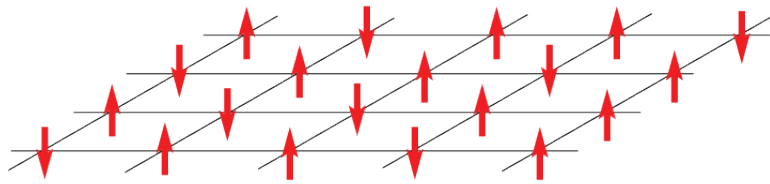
Multidisciplinary drifting Observatory
for the Study of Arctic Climate (**MOSAiC**)

MOSAiC School
aboard the icebreaker *RV Akademik Federov*

September 20 - October 28, 2019

20 grad students from around the world
(3 from U.S., 1 mathematician)

Ising Model for a Ferromagnet



applied magnetic field H

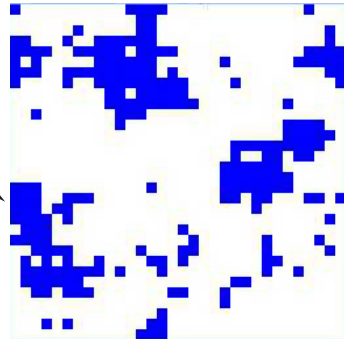
$$s_i = \begin{cases} +1 & \text{spin up} & \text{blue} \\ -1 & \text{spin down} & \text{white} \end{cases}$$

$$\mathcal{H} = -H \sum_i s_i - J \sum_{\langle i,j \rangle} s_i s_j$$

nearest neighbor Ising Hamiltonian

ferromagnetic interaction $J \geq 0$

islands of like spins

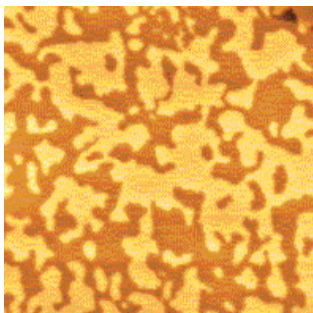


magnetization

homogenized parameter like effective conductivity

$$M(T, H) = \lim_{N \rightarrow \infty} \frac{1}{N} \left\langle \sum_j s_j \right\rangle$$

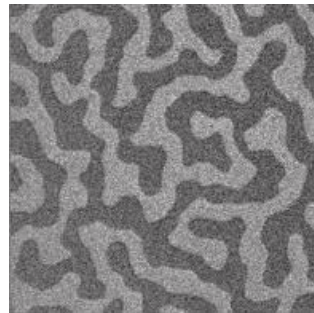
energy is lowered when nearby spins align with each other, forming **magnetic domains**



magnetic domains in cobalt



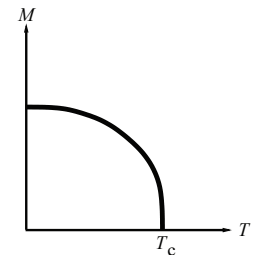
melt ponds (Perovch)



magnetic domains in cobalt-iron-boron



melt ponds (Perovch)



Curie point
critical temperature

Ising model for ferromagnets \longrightarrow Ising model for melt ponds

Ma, Sudakov, Strong, Golden, *New J. Phys.*, 2019

$$\mathcal{H} = - \sum_i^N H_i s_i - J \sum_{\langle i,j \rangle}^N s_i s_j \quad s_i = \begin{cases} \uparrow & +1 \text{ water (spin up)} \\ \downarrow & -1 \text{ ice (spin down)} \end{cases}$$

random magnetic field
represents snow topography

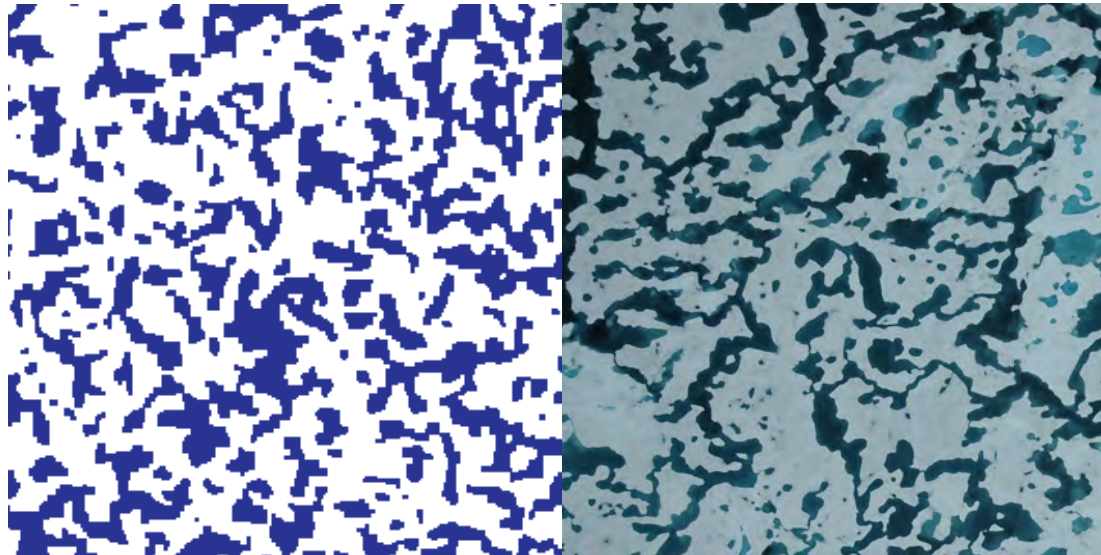
magnetization M

pond coverage $\frac{(M+1)}{2}$
~ albedo

only nearest neighbor
patches interact

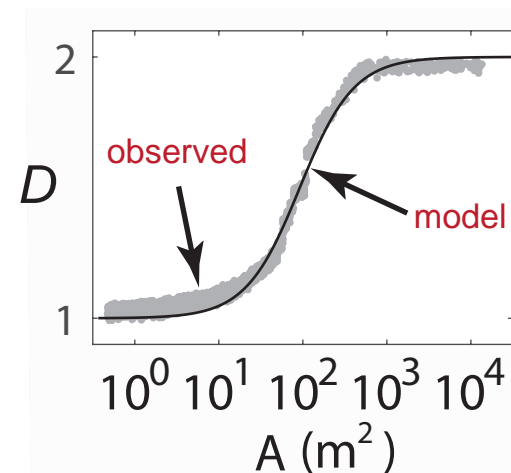
Starting with random initial configurations, as Hamiltonian energy is minimized by Glauber spin flip dynamics, system “flows” toward metastable equilibria.

Order from Disorder



Ising
model

melt pond
photo (Perovich)



pond size
distribution exponent

observed -1.5

(Perovich, et al. 2002)

model -1.58

ONLY MEASURED INPUT = LENGTH SCALE (GRID SIZE) from snow topography data



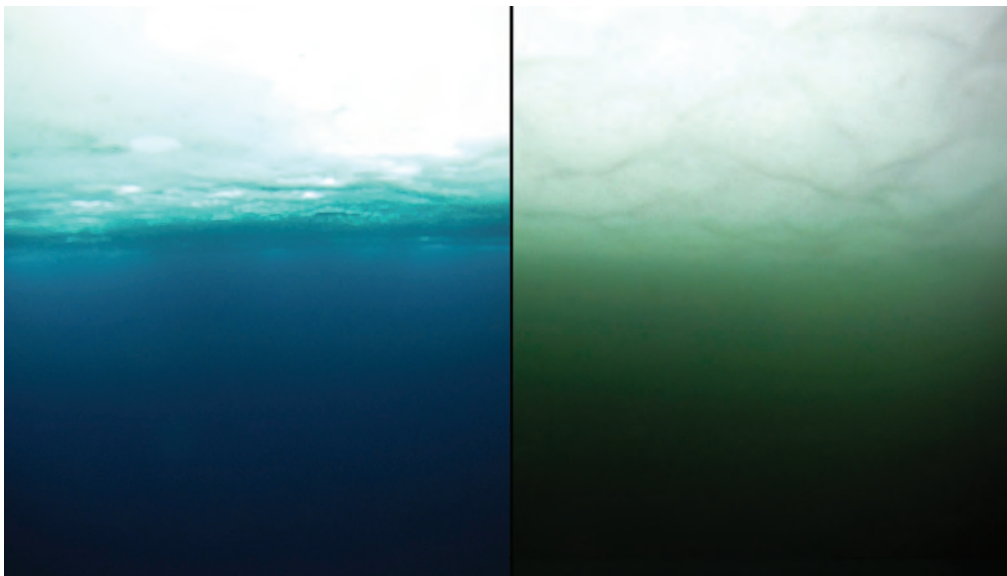
2011 massive under-ice **algal bloom**

Arrigo et al., *Science* 2012

melt ponds act as

WINDOWS

allowing light
through sea ice



no bloom

bloom

***Have we crossed into a
new ecological regime?***

The frequency and extent of sub-ice
phytoplankton blooms in the Arctic Ocean

Horvat, Rees Jones, Iams, Schroeder,
Flocco, Feltham, *Science Advances*, 2017

(2015 AMS MRC, Snowbird)

The effect of melt pond geometry on the distribution of solar energy under first-year sea ice

Horvat, Flocco, Rees Jones, Roach, Golden, *Geophys. Res. Lett.* 2020

- Model for 3D light field under ponded sea ice.
- Distribution of solar energy at depth influenced by *shape and connectivity* of melt ponds, as well as area fraction.
- Aggregate properties of the sub-ice light field, such as a significant enhancement of available solar energy under the ice, are controlled by parameter closely related to pond fractal geometry.
- Model and analysis explain how melt pond geometry *homogenizes* under-ice light field, affecting habitability.

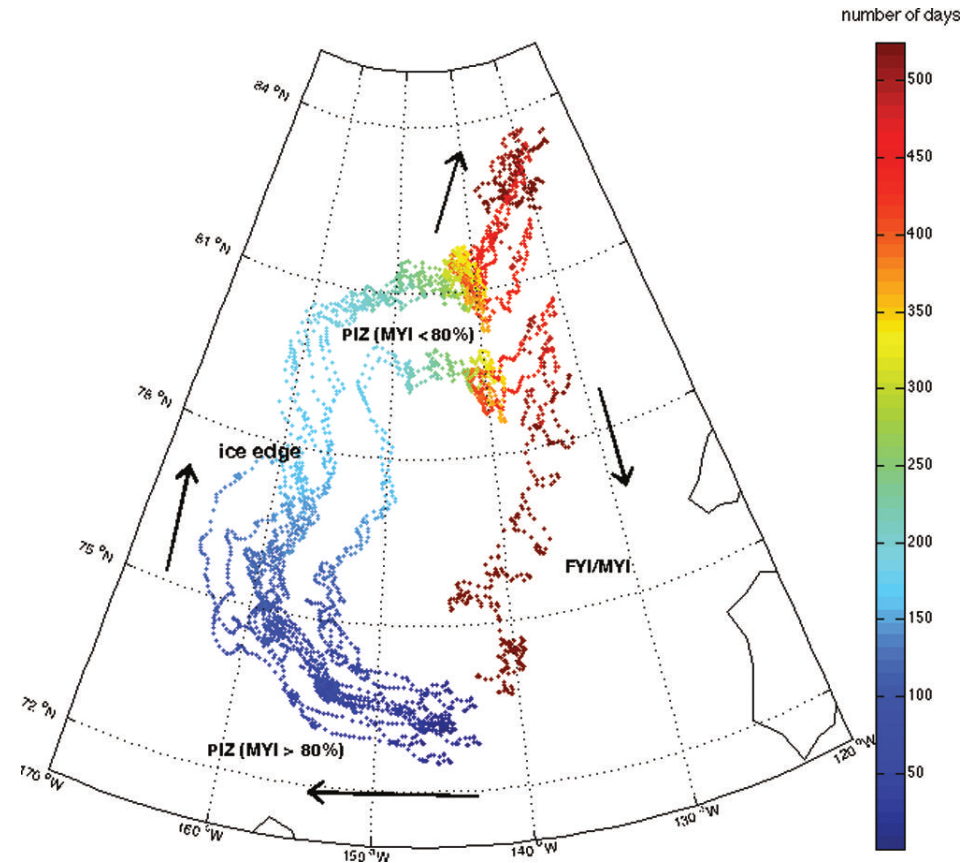
Pond geometry affects ecology and partitioning of solar energy in the upper Arctic Ocean.

macroscale

Anomalous diffusion in sea ice dynamics

Ice floe diffusion in winds and currents

Jennifer Lukovich, Jennifer Hutchings,
David Barber, *Ann. Glac.* 2015



- On short time scales floes observed (buoy data) to exhibit Brownian-like behavior, but they are also being advected by winds and currents.
- Effective behavior is purely diffusive, sub-diffusive or super-diffusive depending on ice pack and advective conditions - **Hurst exponent**.

Floe Scale Model of Anomalous Diffusion in Sea Ice Dynamics

Huy Dinh, Elena Cherkaev, Court Strong, Ken Golden 2020

$$\langle |\mathbf{x}(t) - \mathbf{x}(0) - \langle \mathbf{x}(t) - \mathbf{x}(0) \rangle|^2 \rangle \sim t^\alpha$$

α = Hurst exponent, a measure of anomalous diffusion.

Measured from bouy position data. Detects ice pack crowding and advective forcing.

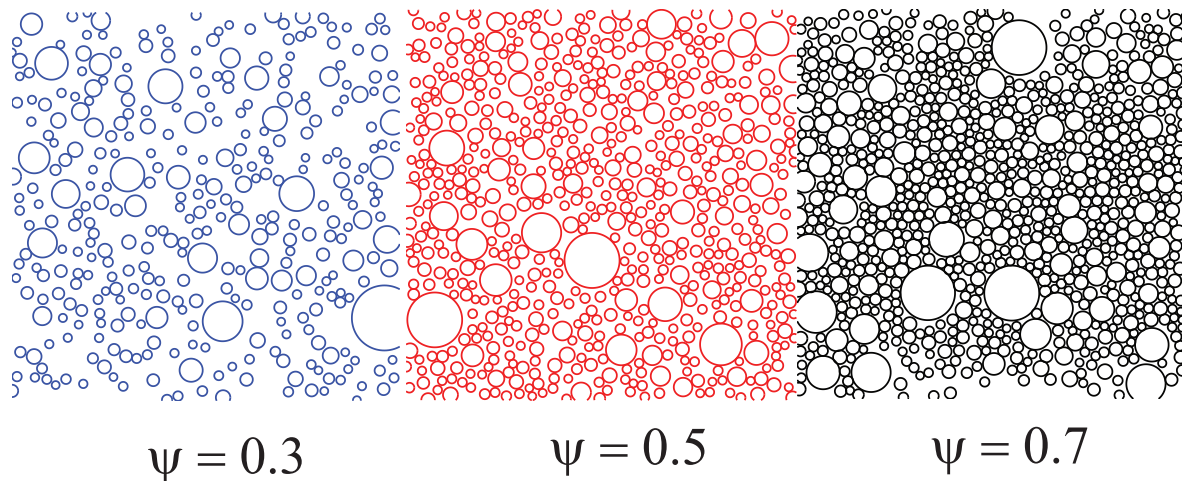
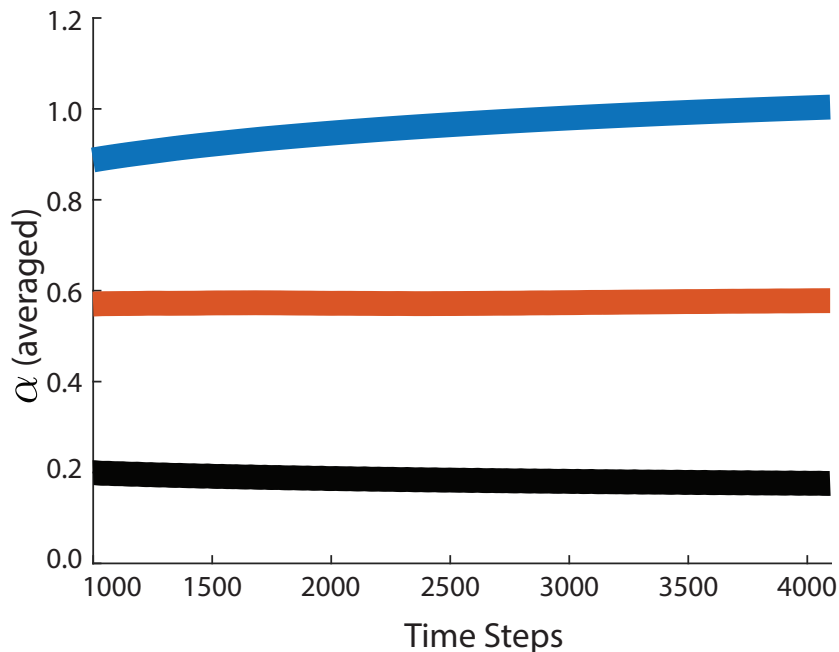
J.V. Lukovich, J.K. Hutchings, D.G. Barber *Annals of Glaciology* 2015

- diffusive** $\alpha = 1$ Sparse packing, uncorrelated advective field.
- sub-diffusive** $\alpha < 1$ Dense packing, crowding dominates advection.
- super-diffusive** $\alpha = 5/4$ Sparse packing, shear dominates advection.
- $\alpha = 5/3$ Sparse packing, vorticity dominates advection.

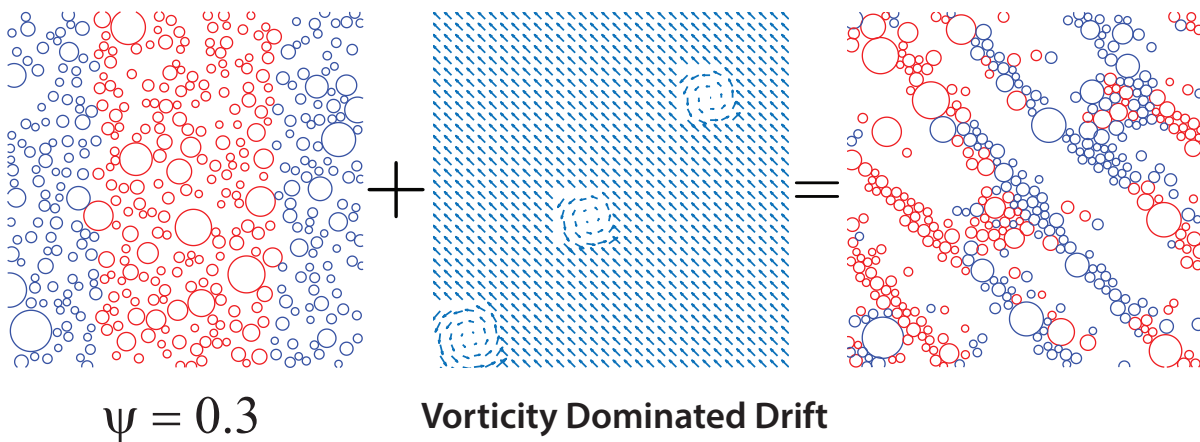
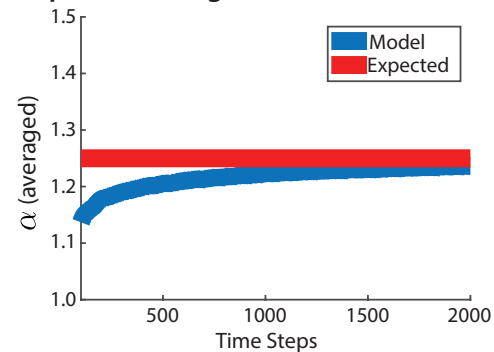
Goal: Develop numerical model to analyze regimes of transport in terms of ice pack crowding and advective conditions.

Model Results

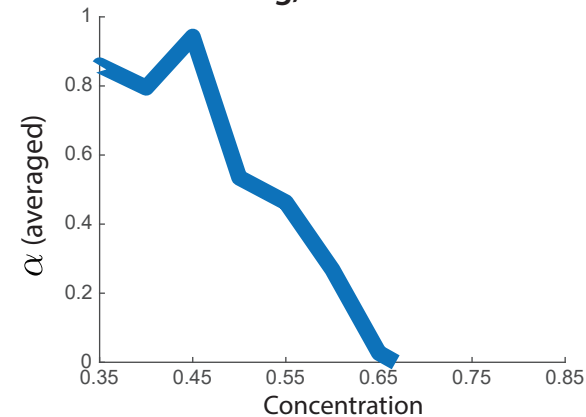
Crowding in Diffusive Drift



Sparse Packing, Shear Dominated Drift



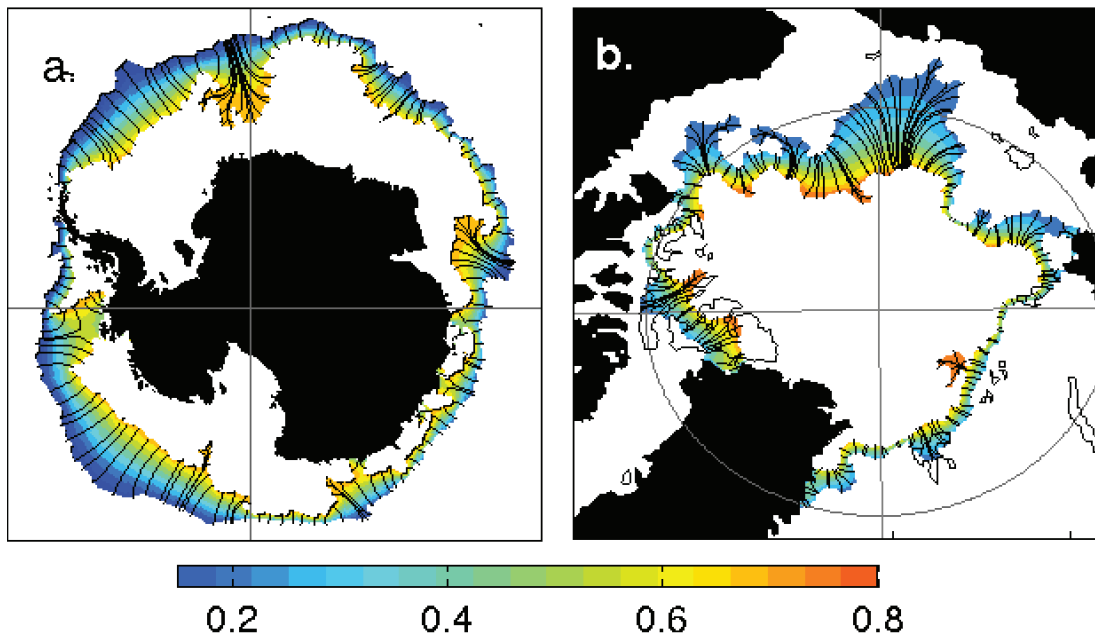
Crowding, Diffusive Drift



Marginal Ice Zone

MIZ

- biologically active region
- intense ocean-sea ice-atmosphere interactions
- region of significant wave-ice interactions



MIZ WIDTH

fundamental length scale of
ecological and climate dynamics

Strong, *Climate Dynamics* 2012

Strong and Rigor, *GRL* 2013

transitional region between
dense interior pack ($c > 80\%$)
sparse outer fringes ($c < 15\%$)

**How to objectively
measure the “width”
of this complex,
non-convex region?**

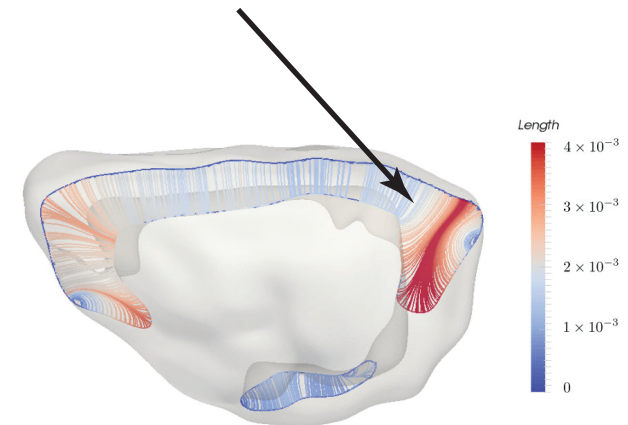
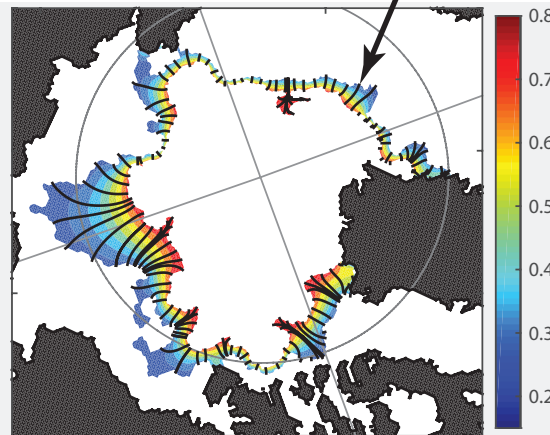
Objective method for measuring MIZ width motivated by medical imaging and diagnostics

Strong, *Climate Dynamics* 2012
Strong and Rigor, *GRL* 2013

39% widening
1979 - 2012

“average” lengths of streamlines

streamlines of a solution
to Laplace’s equation



Arctic Marginal Ice Zone

**cross-section of the
cerebral cortex of a rodent brain**

analysis of different MIZ WIDTH definitions

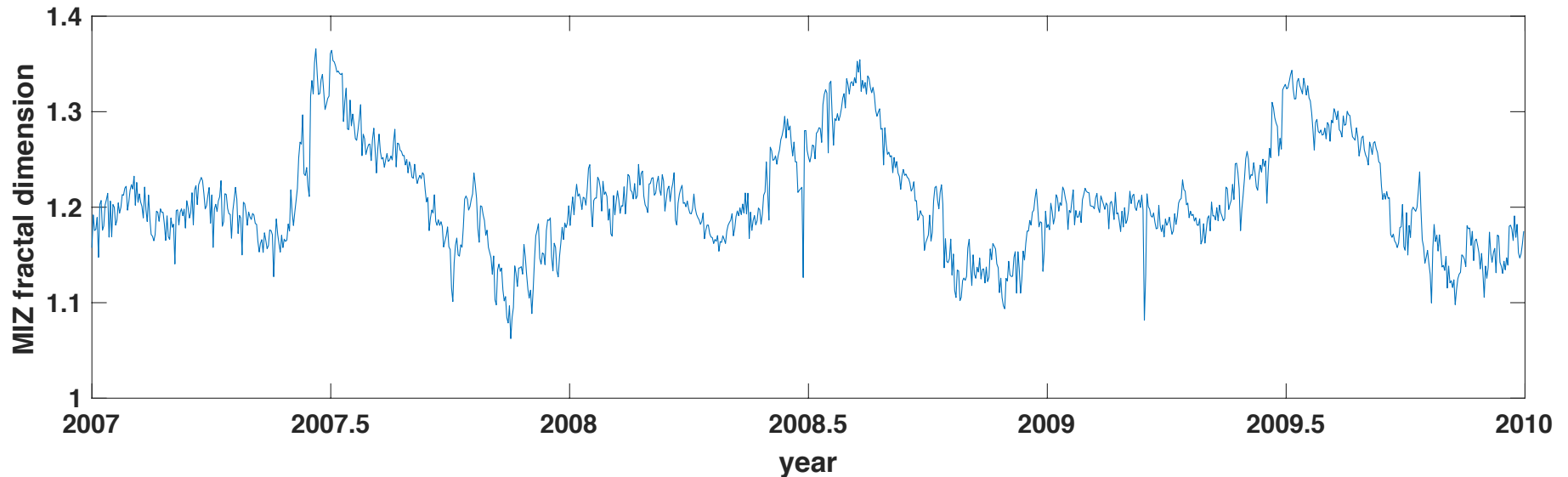
Strong, Foster, Cherkaev, Eisenman, Golden
J. Atmos. Oceanic Tech. 2017

Strong and Golden
Society for Industrial and Applied Mathematics News, April 2017

MIZ fractal dimension

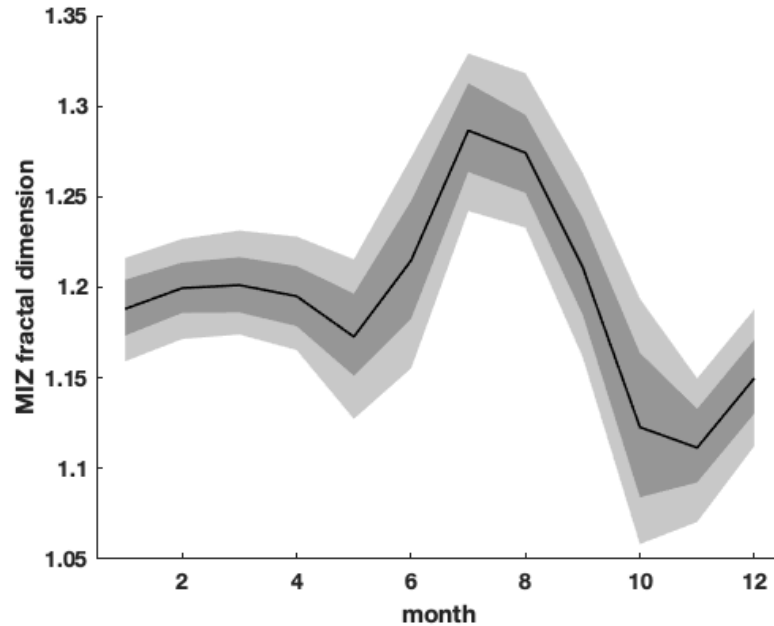
Jerry Zhang, Court Strong, Ken Golden

The shape of the MIZ becomes more complex during the melt season, increasing its fractal dimension.



- MIZ fractal dimension undergoes a pronounced seasonal cycle, maximizing around July
- We have preliminary evidence of decadal trends in MIZ fractal dimension

MIZ fractal dimension



For daily Arctic values 1979-2019
Bold curve: mean
Shading: 10th-90th and 25th-75th
percentiles

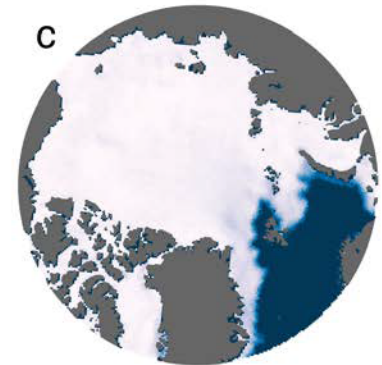
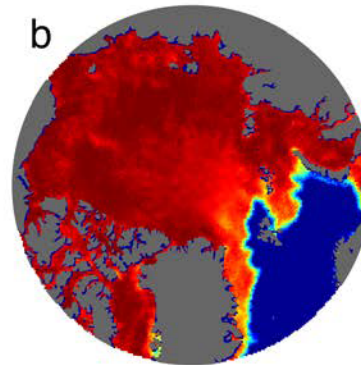
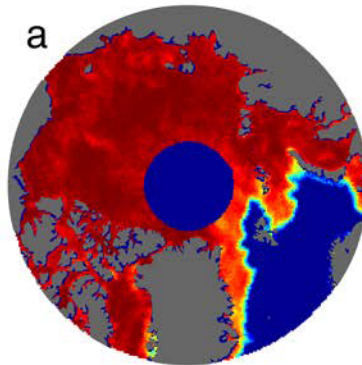
- MIZ fractal dimension undergoes a pronounced seasonal cycle, maximizing around July
- We have preliminary evidence of decadal trends in MIZ fractal dimension

Filling the polar data gap with partial differential equations

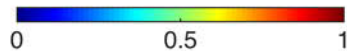
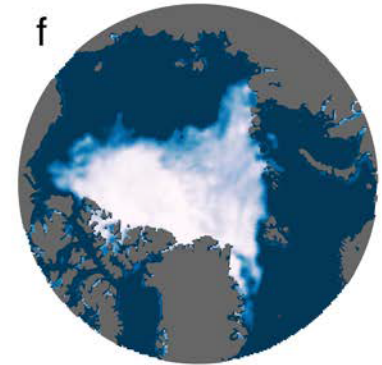
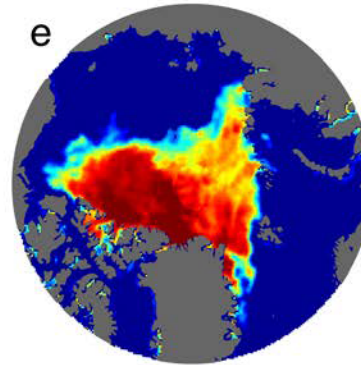
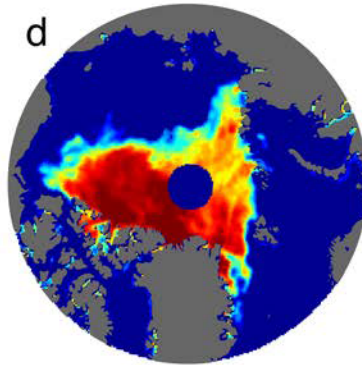
hole in satellite coverage
of sea ice concentration field

previously assumed
ice covered

Gap radius: 611 km
06 January 1985



Gap radius: 311 km
30 August 2007



$$\Delta\psi=0$$

fill with harmonic function satisfying
satellite BC's plus stochastic term

Strong and Golden, *Remote Sensing* 2016
Strong and Golden, *SIAM News* 2017

**NOAA/NSIDC Sea Ice Concentration CDR
product update will use our PDE method.**

University of Utah Sea Ice Modeling Group (2017-2020)

Senior Personnel: Ken Golden, Distinguished Professor of Mathematics
Elena Cherkaev, Professor of Mathematics
Court Strong, Associate Professor of Atmospheric Sciences
Ben Murphy, Ph.D.

Postdoctoral Researcher: Noa Kraitzman (now at Australian National University)

Graduate Students: Kyle Steffen (now at UT Austin with Clint Dawson)
Christian Sampson (now at UNC Chapel Hill with Chris Jones)
Huy Dinh (starting sea ice MURI Postdoc at NYU/Courant)
Rebecca Hardenbrook
David Morison (Physics Department)
Ryleigh Moore
Delaney Mosier, Daniel Hallman

Undergraduate Students: Kenzie McLean, Jacqueline Cinella Rich, Dane Gollero,
Samir Suthar, Anna Hyde, Kitsel Lusted, Ruby Bowers
Kimball Johnston, Jerry Zhang

High School Students: Jeremiah Chapman, Titus Quah, Dylan Webb

Sea Ice Ecology Group Postdoc Jody Reimer, Grad Student Julie Sherman,
Undergrads Anna Hyde, Kayla Stewart + incoming

Conclusions

1. Sea ice is a fascinating multiscale composite with structure similar to many other natural and man-made materials.
2. Mathematical methods developed for sea ice advance the theory of composites and inverse problems in general.
2. **Homogenization and statistical physics help *link scales in sea ice and composites***; provide rigorous methods for finding effective behavior; advance sea ice representations in climate models.
3. **Fluid flow** through sea ice mediates **melt pond evolution** and many processes important to climate change and polar ecosystems.
5. Field experiments are essential to developing relevant mathematics.
6. Our research will help to **improve projections of climate change**, the fate of Earth's sea ice packs, and the ecosystems they support.

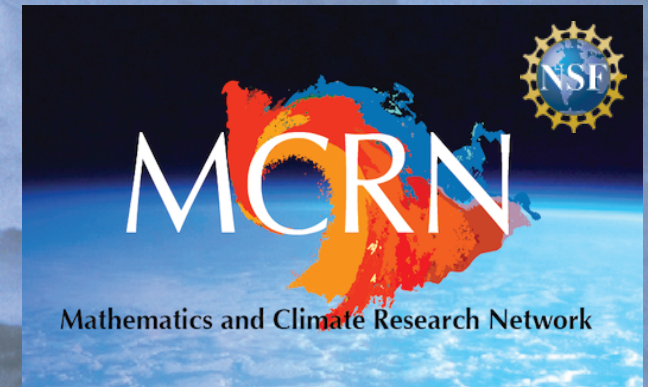
THANK YOU

Office of Naval Research

Applied and Computational Analysis Program
Arctic and Global Prediction Program

National Science Foundation

Division of Mathematical Sciences
Division of Polar Programs



Buchanan Bay, Antarctica Mertz Glacier Polynya Experiment July 1999

ISSN 0002-9920 (print)
ISSN 1088-9477 (online)



Notices

of the American Mathematical Society

November 2020

Volume 67, Number 10



AMERICAN
MATHEMATICAL
SOCIETY

Advancing research. Creating connections.

*The cover is based on "Modeling Sea Ice,"
page 1535.*

Modeling Sea Ice



*Kenneth M. Golden, Luke G. Bennetts,
Elena Cherkhev, Ian Eisenman, Daniel Feltham,
Christopher Horvat, Elizabeth Hunke,
Christopher Jones, Donald K. Perovich,
Pedro Ponte-Castañeda, Courtenay Strong,
Deborah Sulsky, and Andrew J. Wells*

Kenneth M. Golden is a Distinguished Professor of Mathematics at the University of Utah. His email address is golden@math.utah.edu.

Luke G. Bennetts is an associate professor of applied mathematics at the University of Adelaide. His email address is luke.bennetts@adelaide.edu.au.

Elena Cherkhev is a professor of mathematics at the University of Utah. Her email address is elena@math.utah.edu.

Ian Eisenman is an associate professor of climate, atmospheric science, and physical oceanography at the Scripps Institution of Oceanography at the University of California San Diego. His email address is eisenman@ucsd.edu.

Daniel Feltham is a professor of climate physics at the University of Reading. His email address is d.f.feltham@reading.ac.uk.

Christopher Horvat is a NOAA Climate and Global Change Postdoctoral Fellow at the Institute at Brown for Environment and Society at Brown University. His email address is christopher_horvat@brown.edu.

Elizabeth Hunke is a deputy group leader, T-3 fluid dynamics and solid mechanics group at the Los Alamos National Laboratory. Her email address is ec1are@lanl.gov.

Christopher Jones is a Bill Guthridge Distinguished Professor of Mathematics

at the University of North Carolina, Chapel Hill. His email address is ckrtj@unc.edu.

Donald K. Perovich is a professor of engineering at the Thayer School of Engineering at Dartmouth College. His email address is donald.k.perovich@dartmouth.edu.

Pedro Ponte-Castañeda is a Raymond S. Markowitz Faculty Fellow and professor of mechanical engineering and applied mechanics and of mathematics at the University of Pennsylvania. His email address is ponte@seas.upenn.edu.

Courtenay Strong is an associate professor of atmospheric sciences at the University of Utah. His email address is court.strong@utah.edu.

Deborah Sulsky is a professor of mathematics and statistics and of mechanical engineering at the University of New Mexico. Her email address is sulsky@math.unm.edu.

Andrew J. Wells is an associate professor of physical climate science at the University of Oxford. His email address is Andrew.Wells@physics.ox.ac.uk.

Communicated by Notices Associate Editor Reza Malek-Madani.

*For permission to reprint this article, please contact:
reprint-permission@ams.org.*

Special Issue on the Mathematics of Planet Earth

Read about the application of mathematics and computational science to issues concerning invasive populations, Arctic sea ice, insect flight, and more in this Planet Earth special issue!

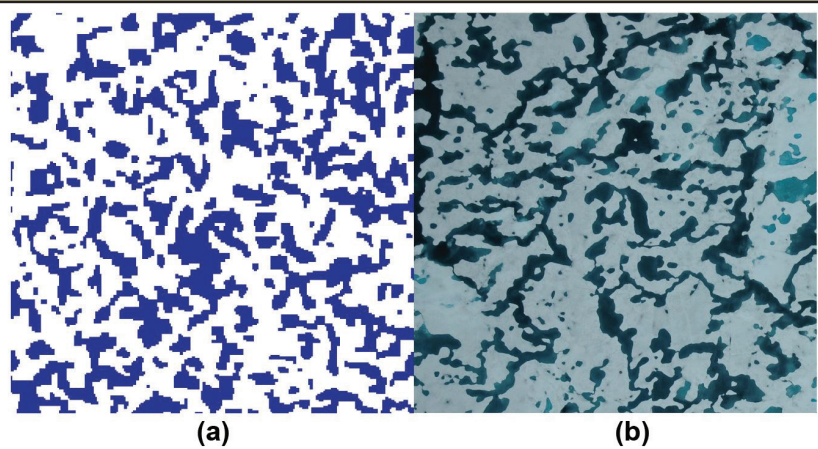


Figure 3. Comparison of real Arctic melt ponds with metastable equilibria in our melt pond Ising model. **3a.** Ising model simulation. **3b.** Real melt pond photo. Figure 3a courtesy of Yiping Ma, 3b courtesy of Donald Perovich.

Vast labyrinthine ponds on the surface of melting Arctic sea ice are key players in the polar climate system and upper ocean ecology. Researchers have adapted the Ising model, which was originally developed to understand magnetic materials, to study the geometry of meltwater's distribution over the sea ice surface. In an article on page 5, Kenneth Golden, Yiping Ma, Courtenay Strong, and Ivan Sudakov explore model predictions.

Controlling Invasive Populations in Rivers

By Yu Jin and Suzanne Lenhart

Flow regimes can change significantly over time and space and strongly impact all levels of river biodiversity, from the individual to the ecosystem. Invasive species in rivers—such as bighead and silver carp, as well as quagga and zebra mussels—continue to cause damage. Management of these species may include targeted adjustment of flow rates in rivers, based on recent research that examines the effects of river morphology and water flow on rivers' ecological statuses. While many previous methodologies rely on habitat suitability models or oversimplification of the hydrodynamics, few studies have focused on the integration of ecological dynamics into water flow assessments.

Earlier work yielded a hybrid modeling approach that directly links river hydrology with stream population models [3]. The hybrid model's hydrodynamic component is based on the water depth in a gradually varying river structure. The model derives the steady advective flow from this structure and relates it to flow features like water discharge, depth, velocity, cross-

sectional area, bottom roughness, bottom slope, and gravitational acceleration. This approach facilitates both theoretical understanding and the generation of quantitative predictions, thus providing a way for scientists to analyze the effects of river fluctuations on population processes.

When a population spreads longitudinally in a one-dimensional (1D) river with spatial heterogeneities in habitat and temporal fluctuations in discharge, the resulting hydrodynamic population model is

$$N_t = -A_t(x,t) \frac{N}{A(x,t)} + \frac{1}{A(x,t)} (D(x,t)A(x,t)N_x)_x - \frac{Q(t)}{A(x,t)} N_x + rN \left(1 - \frac{N}{K}\right)$$

$$\begin{aligned} N(0,t) &= 0 & \text{on } (0,T), x=0, \\ N_x(L,t) &= 0 & \text{on } (0,T), x=L, \\ N(x,0) &= N_0(x) & \text{on } (0,L), t=0 \end{aligned} \quad (1)$$

See *Invasive Populations* on page 4

Modeling Resource Demands and Constraints for COVID-19 Intervention Strategies

By Erin C.S. Acquesta, Walt Beyeler, Pat Finley, Katherine Klise, Monear Makvandi, and Emma Stanislawski

As the world desperately attempts to control the spread of COVID-19, the need for a model that accounts for realistic trade-offs between time, resources, and corresponding epidemiological implications is apparent. Some early mathematical models of the outbreak compared trade-offs for non-pharmaceutical interventions [3], while others derived the necessary level of test coverage for case-based interventions [4] and demonstrated the value of prioritized testing for close contacts [7].

Isolated analyses provide valuable insights, but real-world intervention strategies are interconnected. Contact tracing is the lynchpin of infection control [6] and forms the basis of prioritized testing. Therefore, quantifying the effectiveness of contact tracing is crucial to understanding the real-life implications of disease control strategies.

Contact Tracing Demands

Contact tracers are skilled, culturally competent interviewers who apply their knowledge of disease and risk factors when notifying people who have come into contact with COVID-19-infected individuals. They also continue to monitor the situation after case investigations [1].

Case investigation consists of four steps:

1. Identify and notify cases
2. Interview cases
3. Locate and notify contacts
4. Monitor contacts.

Most health departments are implementing case investigation, contact identification, and quarantine to disrupt COVID-19 transmission. The timeliness of contact tracing is constrained by the length of the infectious period, the turn-around time for testing and result reporting, and the ability to successfully reach and interview patients and their contacts. The European Centre for Disease Prevention and Control approximates that contact tracers spend one to two hours conducting an interview [2]. Estimates regarding the timelines of other steps are limited to subject matter expert elicitation and can vary based on cases' access to phone service or willingness to participate in interviews.

Bounded Exponential

The fundamental structure of our model follows traditional susceptible-exposed-infected-recovered (SEIR) compartmental modeling [5]. We add an asymptomatic population A , a hospitalized population H , and disease-related deaths D , as well as corresponding quarantine states. We define the states $\{S_i, E_i, A_i, I_i, H, R, D\}_{i=0,1}$ for our compartments, such that $i=0$ and $i=1$

correspond to unquarantined and quarantined respectively. Rather than focus on the dynamics that are associated with the state transition diagram in Figure 1, we introduce a formulation for the real-time demands on contact tracers' time as a function of infection prevalence, while also respecting constraints on resources.

When the work that is required to investigate new cases and monitor existing contacts exceeds available resources, a backlog develops. To simulate this backlog, we introduce a new compartment C for tracking the dynamic states of cases:

$$\frac{dC}{dt} = [flow_{in}] - [flow_{out}].$$

Flow into the backlog compartment, represented by $[flow_{in}]$, reflects case identification that is associated with the following transitions in the model:

- The rate of random testing: $q_{rA}(t)A_0(t) \rightarrow A_1(t)$ and $q_{rI}(t)I_0(t) \rightarrow I_1(t)$
- Testing triggered by contact tracing: $q_{tA}(t)A_0(t) \rightarrow A_1(t)$, $q_{tI}(t)I_0(t) \rightarrow I_1(t)$, and $q_{tE}(t)E_1(t) \rightarrow \{A_1(t), I_1(t)\}$
- The population that was missed by the non-pharmaceutical interventions that require hospitalization: $\tau_{IH}(t)I_0(t) \rightarrow H(t)$.

Here, $q_{rA}(t)$ defines the time-dependent rate of random testing, $q_{tA}(t)$ signifies the time-dependent rate of testing that is triggered by contact tracing, and τ_{IH} is the inverse of the expected amount of time for which an infected individual is symptomatic before hospitalization. These terms collectively provide the simulated number of newly-identified positive COVID-19 cases. However, we also need the average number of contacts per case. We thus define function $\mathcal{K}(\kappa, T_S, \phi_\kappa)$ that depends on the average number of contacts a day (κ), the average number of days for which an individual is infectious before going into isolation (T_S), and the likelihood that the individual

See *COVID-19 Intervention* on page 3

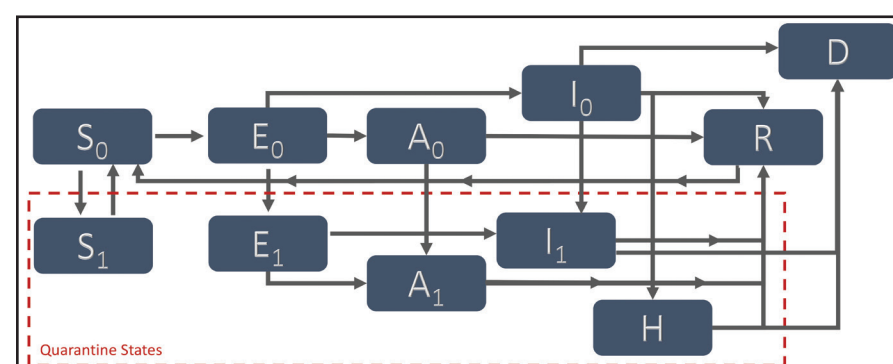
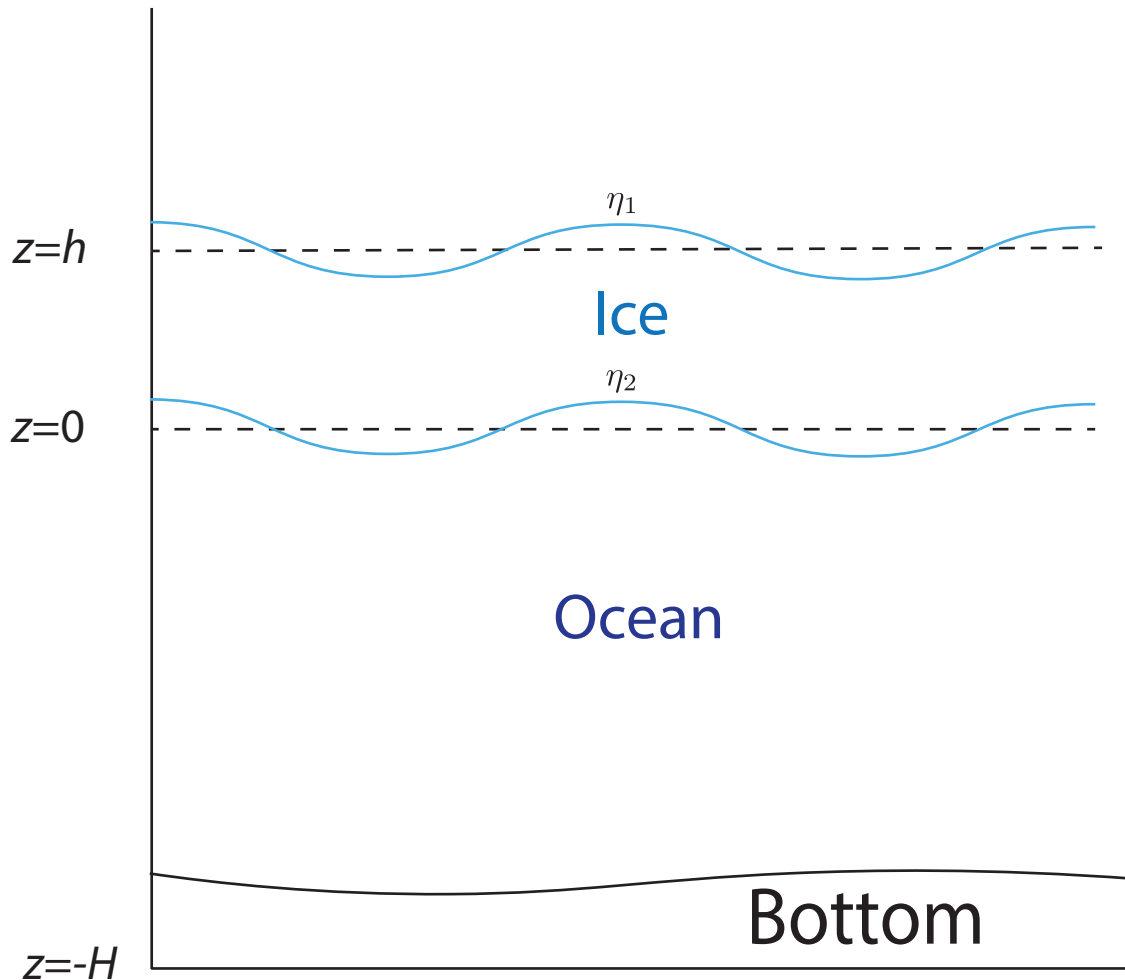


Figure 1. Disease state diagram for the compartmental infectious disease model. Figure courtesy of the authors.

Nonprofit Org
U.S. Postage
PAID
Permit No 360
Bellmawr, NJ

siam
SOCIETY for INDUSTRIAL and APPLIED MATHEMATICS
3600 Market Street, 6th Floor
Philadelphia, PA 19104-2688 USA

Two Layer Models and Effective Rheological Parameters



Viscous fluid layer (Keller 1998)

\tilde{E} effective Viscosity ν

Equations of motion:
$$\frac{\partial U}{\partial t} = -\frac{1}{\rho} \nabla P + \nu \nabla^2 U + g$$

Viscoelastic fluid layer (Wang-Shen 2010)

\tilde{E} effective Complex Viscosity $\nu_e = \nu + iG/\rho\omega$

Equations of motion
$$\frac{\partial U}{\partial t} = -\frac{1}{\rho} \nabla P + \nu_e \nabla^2 U + g$$

Viscoelastic thin beam (Mosig *et al.* 2015)

\tilde{E} effective Complex Shear Modulus $G_v = G - i\omega\rho\nu$

Stieltjes integral representation for effective complex viscoelastic parameter; bounds

Sampson, Murphy, Cherkaev, Golden 2019

G shear modulus P pressure ω angular frequency U velocity field
 ν viscosity λ Poission ratio ρ density g gravity

Homogenization for two phase viscoelastic composite

microscale $\sigma = C_{ijkl}\epsilon_{kl} = C:\epsilon$

macroscale $\langle \sigma \rangle = C^*:\langle \epsilon \rangle$

$$\langle \epsilon \rangle = \epsilon^0$$

quasistatic assumption $\nabla \cdot \sigma = 0$

Resolvent

$$\epsilon = \left(1 - \frac{1}{s}\Gamma\chi_1\right)^{-1} \epsilon^0 \quad \rightarrow \quad \frac{v^*}{v_2} = \left(1 - \|\epsilon^0\|^{-2}F(s)\right)$$

$$\Gamma = \nabla^S (\nabla \cdot \nabla^S)^{-1} \nabla \cdot$$

$$v_1 = 10^7 + i4875 \quad \text{pancake ice}$$

$$v_2 = 5 + i0.0975 \quad \text{slush / frazil}$$

$$C = 2(\chi_1 v_1 + \chi_2 v_2)\Lambda_s$$



Strain Field

$$\epsilon = \frac{1}{2} [\nabla u + (\nabla u)^T] = \nabla^S u \quad \nabla \cdot u = 0$$

$$F(s) = \int_0^1 \frac{d\mu(\lambda)}{s - \lambda} \quad s = \frac{1}{1 - \frac{v_1}{v_2}}$$

Model Approximations

Floes \approx Discs

$$\text{Forces on Disc} = F_{drag} + F_{collision}$$

A. Herman *Physical Review E* 2011

Floe-Floe Interactions: Linear Elastic Collisions

$F_{collision}$ follows Hooke's Law.

Advective Forcing: Passive, Linear Drag Law

v is the advective velocity field.

F_{drag} is proportional to relative velocity.

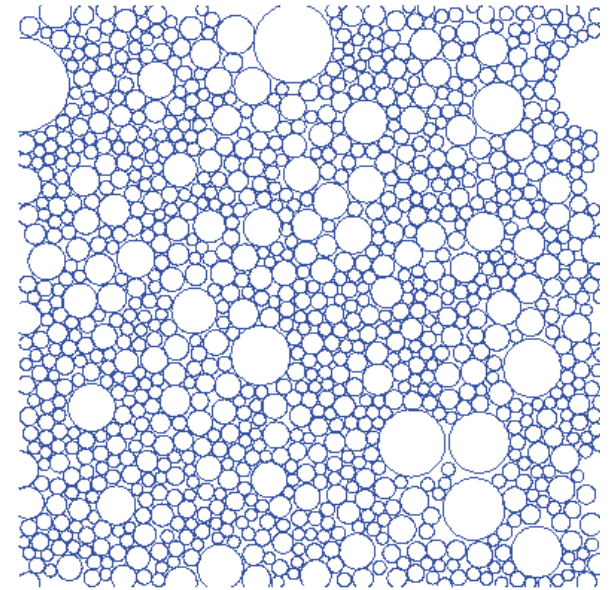
Ice Pack Characteristics

ϕ = sea ice concentration (floe area fraction)

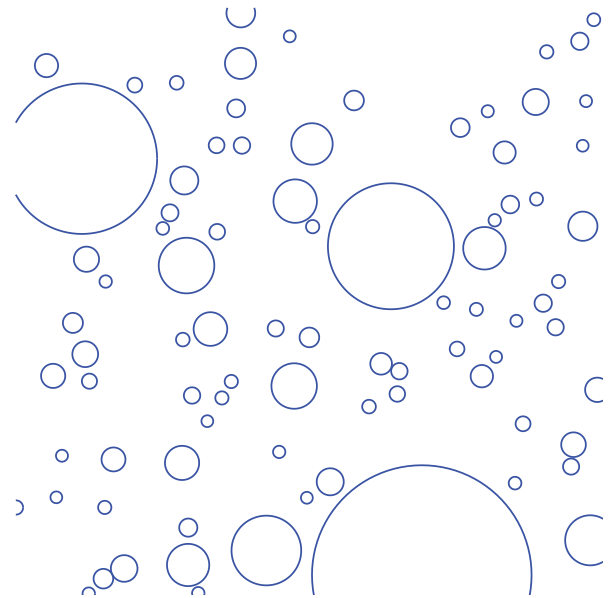
Power Law Size Distribution: $N(D) \sim D^{-k}$

T. Toyota, S. Takatsuji, M. Nakayama *Geophysical Review Letters* 2006

k = floe diameter exponent



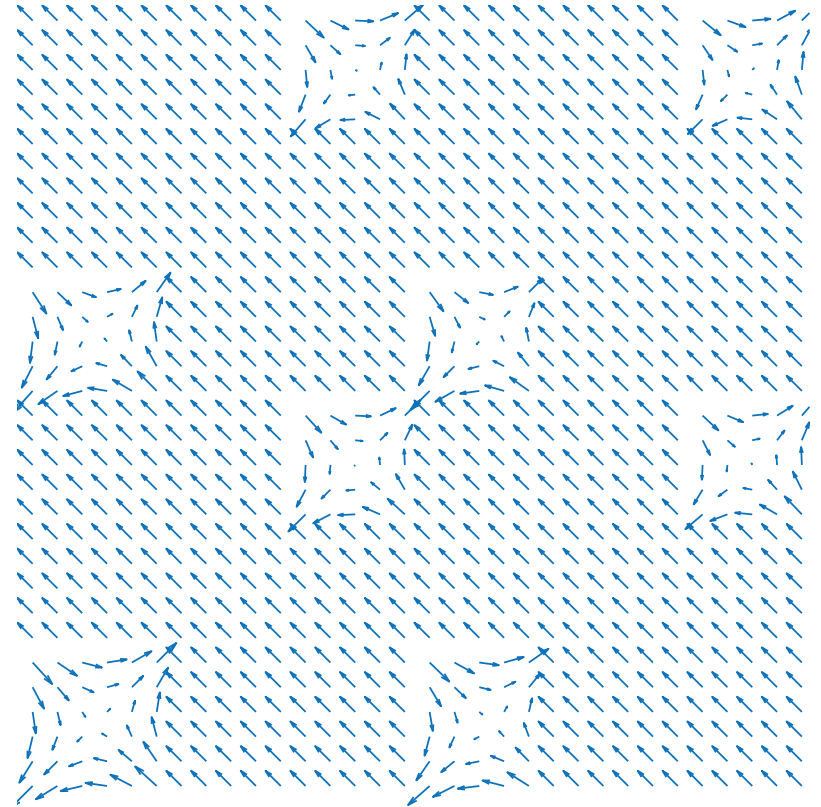
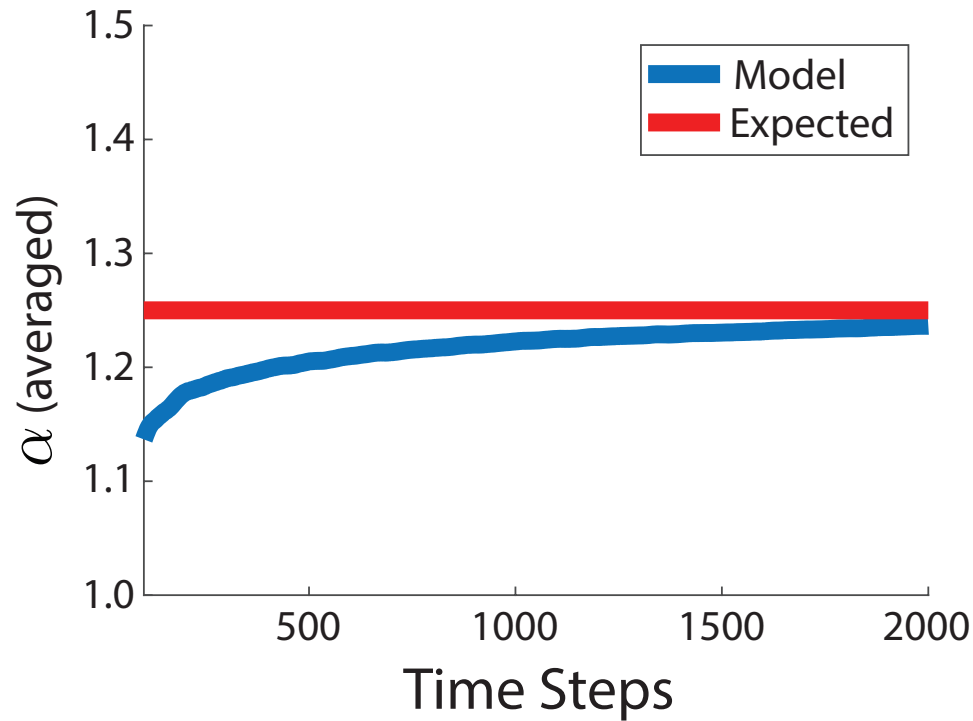
$$k = 2.9, \phi = 0.8$$



$$k = 1.7, \phi = 0.1$$

Model Results

Sparse Packing, Shear Dominated Drift



Expected $\alpha = 5/4$

$k = 2.9$ Concentration = 0.3